AD NUMBER

AD068499

NEW LIMITATION CHANGE

TO

Approved for public release, distribution unlimited

FROM

Distribution authorized to U.S. Gov't. agencies and their contractors; Administrative/Operational Use; 01 MAR 1955. Other requests shall be referred to Naval Ordnance Laboratory, White Oak, MD.

AUTHORITY

USNOL ltr dtd 29 aug 1974

NAVORD REPORT 3880

FC

NOL HYPERSONIC TUNNEL NO. 4 RESULTS VII: EXPERIMENTAL INVESTIGATION OF TURBULENT BOUNDARY LAYERS IN HYPERSONIC FLOW

1 MARCH 1955

U. S. NAVAL ORDNANCE LABORATORY
WHITE OAK, MARYLAND

NAVORD Report 3880

Aeroballistic Research Report 262

NOL HYPERSONIC TUNNEL NO. 4 RESULTS VII: EXPERIMENTAL INVESTIGATION OF TURBULENT BOUNDARY LAYERS IN HYPERSONIC FLOW

Prepared by:

R. Kenneth Lobb, Eva M. Winkler, and Jerome Persh

ABSTRACT: Naturally turbulent boundary layers on the wall of a wedge-type water-cooled nozzle in the NOL 12 x 12 cm Hypersonic Tunnel No. 4 have been investigated at Mach numbers of 5.0 to 8.2 with and without steady state heat transfer to the surface. The Reynolds number based on boundary layer momentum thickness was varied from 5,000 to 13,000. Measurements of Pitot and static pressures, total and wall temperatures, and rates of heat transfer made it possible to compute velocity profiles, temperature profiles, and boundary layer parameters without resorting to any assumptions. The turbulent portion of the boundary layer velocity profile was found to differ from the incompressible flow logarithmic law by an amount that depends on the heat transfer and Mach number. The data for the outer turbulent portion for any one Mach number fall on a single curve if plotted in a particular nondimensional coordinate system which is based on local properties in the boundary layer. The velocity profile in the laminar sublayer is linear. The thermal sublayer was found in all cases to be larger than the velocity sublayer. Local skin friction coefficients for zero heat transfer as calculated from the velocity gradients at the wall are consistent with the results of other experimenters at lower Mach numbers for the same Reynolds number. Furthermore it is demonstrated that the Reynolds analogy between skin friction and heat transfer is valid at Mach numbers up to 8.2.

U. S. NAVAL ORDNANCE LABORATORY
WHITE OAK, MARYLAND

This is the seventh NAVORD Report on an investigation carried out in the continuous NOL 12 x 12 cm Hypersonic Tunnel No. 4. The titles of the previous NAVORD's describing results from the tunnel are:

I. Air Liquefaction. NAVORD 1742, 4 January 1951

II. Diffuser Investigation. NAVORD 2376, 5 May 1952

III. Diffuser Investigation with Models and Support. NAVORD 2435, 1 July 1952

IV. High Supply Temperature Measurement and Control. NAVORD 2574, 8 October 1952

V. Experimental and Theoretical Investigation of a Cooled Hypersonic Wedge Nozzle. NAVORD 2701, 13 April 1953

VI. Experimental and Theoretical Investigation of the Boundary Layer and Heat Transfer Characteristics of a Cooled Hypersonic Wedge Nozzle at a Mach Number of 5.5. NAVORD 3757, 8 July 1954

The present NAVORD (Results VII) presents experimental investigations and discussions of turbulent boundary layers in hypersonic flow.

Knowledge of the related effect of skin friction and aerodynamic heating at high Mach numbers is needed by the designers of hypersonic vehicles because, for slender missiles, skin friction represents the major part of the drag and extreme surface temperatures produced by frictional heating may very well be a limiting design factor.

A portion of the results contained in this NAVORD were presented at the 22nd Annual Meeting of the Institute of Aeronautical Sciences and also at the Bureau of Ordnance Committee on Aeroballistics Symposium in October 1954. The present report contains additional results and more detailed analysis of the data as well as a complete tabulation of the experimental results.

This work was jointly sponsored by the U. S. Naval Bureau of Ordnance and the U. S. Air Force. It was carried out under Tasks NOL-M9a-108-1-54, NOL-M9a-133-1-55, and NOL-M9a-133-5-55.

The authors are indebted to Dr. R. E. Wilson for many stimulating discussions during the course of the investigations.

The numerical evaluation of the boundary layer surveys was done on a card-programmed calculator of the Applied Mathematics Division. The preparation of the data for the card-programmed calculator was greatly assisted by Dr. E. K. Blum. The cooperation of Messrs. L. L. Liccini and R. Carren, Jr., who participated during the tests, is acknowledged.

JOHN T. HAYWARD
Captain, USN
Commander

H. H. KURZWEG, Chief
Aeroballistic Research Department
By direction

CONTENTS

	Page
Introduction	1
Experimental Equipment and Techniques	1
Data Reduction	3
ults	5
Boundary Layer Profiles	5
Nondimensional Velocity Profile Representation	7
Velocity and Thermal Sublayers	8
Discussion of Skin Friction Data	9
Concluding Remarks	11
References	13
Appendix A, Tabulation of Experimental Data	15

ILLUSTRATIONS

		Page
Figure 1.	NOL 12 x 12 cm Hypersonic Tunnel	23
Figure 2.	Temperature and Pressure Probes	24
Figure 3.	Mach Number Variation Across Boundary Layer for Free-Stream Mach Numbers of 5.0 and 6.8 and Various Rates of Heat Transfer	25
Figure 4.	Stagnation Temperature Variation Across Boundary Layer for Free-Stream Mach Numbers of 5.0 and 6.8 and Various Rates of Heat Transfer	26
Figure 5.	Static Temperature Variation Across Boundary Layer for Free-Stream Mach Numbers of 5.0 and 6.8 and Various Rates of Heat Transfer	27
Figure 6.	Velocity Variation Across Boundary Layer for Free-Stream Mach Numbers of 5.0 and 6.8 and Various Rates of Heat Transfer	28
Figure 7.	Variation of $(\overline{u'^2}/u^2)^{\frac{1}{2}}$ with Wall Distance Parameter	29
Figure 8.	Semi-Logarithmic Representation of Boundary Layer Velocity Profile for a Free-Stream Mach Number of 5.0 and Four Rates of Heat Transfer	30
Figure 9.	Semi-Logarithmic Representation of Boundary Layer Velocity Profile for a Free-Stream Mach Number of 5.8 and Three Rates of Heat Transfer	31
Figure 10.	Semi-Logarithmic Representation of Boundary Layer Velocity Profile for a Free-Stream Mach Number of 6.8 and Four Rates of Heat Transfer	32
Figure 11.	Semi-Logarithmic Representation of Boundary Layer Velocity Profile for Free-Stream Mach Numbers of 7.7 and 8.2	33
Figure 12.	Semi-Logarithmic Representation of Turbulent Portion of Boundary Layer Profiles in u^*, y^*/H Coordinates for Various Mach Numbers	34
Figure 13.	Variation of u^* with Mach Number for Various Values of y^*/H	35
Figure 14.	Logarithmic Representation of Boundary Layer Velocity Profiles	36
Figure 15.	Variation of Skin Friction Ratio with Heat Transfer Parameter	37
Figure 16.	Variation of $u_L^+ = y_L^+$ Values with Heat Transfer Parameter	38
Figure 17.	Variation of Skin Friction Coefficients with Mach Number for Zero Heat Transfer and a Re_θ Value of 5,000	39

SYMBOLS

c_f local skin friction coefficient based on free-stream conditions $\frac{2\tau_w}{\rho_\infty u_\infty^2}$

c_{fi} incompressible local skin friction coefficient for zero heat transfer based on free-stream conditions

c_p specific heat at constant pressure

H boundary layer shape parameter δ^*/θ

k thermal conductivity

M Mach number

Nu Nusselt number for stagnation temperature probe

Pr Prandtl number

p_o stagnation pressure

p'_o Pitot pressure

p static pressure

R Gas constant

Re Reynolds number based on free-stream conditions

r recovery factor

St Stanton number (equation (3))

T'_o local stagnation temperature

T_i stagnation temperature as measured by a stagnation temperature probe

T local static temperature

u velocity

u' velocity component perpendicular to wall

u_τ friction velocity $(\tau_w/\rho)^{\frac{1}{2}}$

u^+ velocity parameter u/u_τ (ρ based on wall properties)

u^* velocity parameter u/u_τ (ρ based on local properties)

y distance perpendicular to wall

y^+ wall distance parameter $y\, u_\tau / \nu$ (ρ and ν based on wall properties)

y^* wall distance parameter $y\, u_\tau / \nu$ (ρ and ν based on local properties)

γ ratio of specific heats

δ total boundary layer thickness

δ^* boundary layer displacement thickness $\int_0^\delta \left[1 - \frac{\rho\, u}{\rho_\infty u_\infty}\right] dy$

θ momentum thickness $\int_0^\delta \frac{\rho\, u}{\rho_\infty u_\infty}\left[1 - \frac{u}{u_\infty}\right] dy$

μ viscosity

ν kinematic viscosity

ρ density

τ shear stress

Subscripts

e equilibrium wall temperature for zero heat transfer

g physical properties of gas

L edge of laminar sublayer

p temperature probe

t physical properties of thermocouple wire

T temperature profile

u velocity profile

w values based on wall conditions

θ values based on momentum thickness

∞ values based on free-stream conditions outside boundary layer

2 conditions behind shock in front of probe

NAVORD Report 3880

NOL HYPERSONIC TUNNEL NO. 4 RESULTS VII: EXPERIMENTAL INVESTIGATION OF TURBULENT BOUNDARY LAYERS IN HYPERSONIC FLOW

INTRODUCTION

1. Boundary layer investigations at hypersonic speeds are of immediate practical interest since friction drag and heat transfer data are needed by the designers of hypersonic missiles.

2. From the theoretical viewpoint, various treatments of the problem are available for the case of laminar boundary layer flows as well as for turbulent boundary layers. The experimental data are, however, limited, and in general cover the Mach number range up to about 5. The lack of experimental confirmation for laminar boundary layer theory is not regarded as serious since the theory is considered to be more or less exact. Most of the analyses of compressible turbulent boundary layer flows, however, are based on experimental results obtained in wholly incompressible flow. The uncertainties in these analyses have led to large discrepancies in the prediction of skin friction and heat transfer. Even those theories which agree with each other and with the existing experimental data within 5 percent up to Mach numbers of 5 differ greatly at hypersonic Mach numbers (reference (a)).

3. The purpose of the present investigation was to extend the Mach number range of available data and also to attempt to provide a deeper insight into the characteristics of a turbulent boundary layer in compressible flows.

Experimental Equipment and Techniques

4. The boundary layer surveys have been conducted in the NOL 12 x 12 cm Hypersonic Tunnel No. 4, which is described in references (b), (c), and (d). This tunnel operates continuously in the Mach number range from 5 to 10 free of air condensation effects. Supply temperatures from 300 to 800° K and supply pressures from 1 to 15 atmospheres are available. A two-dimensional water-cooled wedge nozzle expands the air and can be adjusted for any Mach number simply by changing the throat opening area.

5. The investigations were made for a range of Mach numbers varying from 5 to about 8. For each Mach number several surveys were made differing in the Reynolds number and the rate of heat transfer to the wall. The surveys were made at the center of one nozzle wall, approximately four inches upstream of the nozzle exit plane, Figure 1. Measurements at this position are unaffected by the junction of the nozzle

end and the first diffuser plate (reference (e)). The relatively thick (approximately 25 mm) turbulent boundary layer on the nozzle wall minimizes probe positioning errors and thus facilitates accurate determination of the profile shapes. Such a boundary layer, however, is subjected to a slight free-stream pressure gradient in the neighborhood of the survey station because the flow is radial. (The corresponding Mach number rise is about 3 percent per tunnel caliber at the survey plane for a Mach number of 5 and decreases with increasing Mach number.) It is felt that the effect of the pressure gradient on the profiles is small. The wall temperature, on the other hand, is maintained practically constant near room temperature over the entire length of the nozzle, except at the throat where the surface temperature approaches the recovery temperature. In all tests the transition from laminar to turbulent boundary layer occurred slightly downstream of the nozzle throat*. The exact effect of the history on the local boundary layer characteristics is, of course, not fully known and the results must be interpreted with this fact in mind.

6. Reynolds numbers and the rate of heat transfer to the wall are controlled by the supply pressure and the supply temperature. In all tests the Reynolds numbers based on boundary layer thickness are roughly two orders of magnitude greater than needed to make slip flow effects at the surface negligible (reference (f)). Since the wall temperature is always maintained near room temperature, the lowest rate of heat transfer to the water-cooled nozzle that could be realized corresponds to a supply temperature which is just high enough to avoid air condensation in the test section.

7. For each survey, Pitot and static pressures, stagnation and wall temperatures, and the wall temperature gradient perpendicular to the nozzle surface are recorded. Static pressures are measured by a 0.64 mm diameter orifice in the wall and by a static probe in the free stream just outside the edge of the boundary layer. The static probe is an 8° cone cylinder with orifices located 17 diameters aft of the shoulder, Figure 2. It is mounted from the side wall with its axis parallel to the flow. Since agreement between wall- and free-stream static pressures is within 1 percent, a constant static pressure has been assumed to exist through the boundary layer. The measurements are made with silicone oil manometers of ± 2 microns measuring accuracy.

---

*Surface probe tests made subsequent to the results reported in reference (e) indicated that the boundary layer profile reported in this reference was close to the transition region. It was definitely established, from the results of the surface probe tests, that all boundary layer profiles presented herein were measured in the fully turbulent region.

8. The Pitot pressure is surveyed from wall to free stream with a flattened hypodermic tube of 0.125 mm half height, Figure 2. The opening is large enough to avoid errors due to slip flow effects on the pressure measurements in the region of low Reynolds number in the boundary layer near the wall (reference (g)). The probe is mounted in a micro-traverse mechanism which also accommodates the connection to the pressure gauge. The position of the centerline of the probe is measured relative to the position of electrical contact between probe and wall with an accuracy of $\pm$ 0.025 mm. Impact pressures above 20 mm Hg are measured with a precision mercury manometer of $\pm$ 0.1 mm measuring accuracy. For the lower pressures a silicone oil manometer is used.

9. A stagnation temperature probe with a single platinum-coated silica shield is used for the temperature surveys of the boundary layer, Figure 2 (reference (h)). For the measurements close to the wall, a flattened probe with a half height of 0.48 mm is used. The temperature recovery factor of the probes reaches a value of 0.998 for large Reynolds numbers. The variation of the temperature recovery factor with flow parameters for each probe is described by a single calibration curve by relating the calibration data to the flow conditions inside the probe. Reference to this curve makes it possible to determine accurately total and static temperatures throughout the boundary layer from measured temperatures and pressures. The e.m.f. output of the temperature probe is recorded on Brown temperature recorders. The temperature measurements are accurate to $\pm 0.2^{\circ}$ C.

10. Local values of the heat transfer to the nozzle wall and nozzle surface temperatures at the boundary layer survey station are obtained from temperature measurements in the nozzle wall. These measurements are made with four thermo-couples imbedded in the nozzle wall at various distances from the surface (reference (d)). Depending upon the operational conditions of the tunnel and the rate of coolant flow to the nozzle, equilibrium readings are reached after 10 to 20 minutes of tunnel operation. They show that the temperature drops linearly from the nozzle surface. Previous investigations indicate that longitudinal and lateral temperature gradients at the nozzle surface can be neglected (reference (d)). The wall temperatures are measured to within $\pm 0.01^{\circ}$ C with a Leeds and Northrup K-2 type potentiometer.

Data Reduction

11. The experimental data needed to evaluate the boundary layer profiles are:

a. Pitot pressure, p_o', vs. distance from wall

b. Static pressure, p, taken constant

c. Measured total temperature, T_i, vs. distance from wall

d. Variation of probe temperature recovery factor with flow parameters

Since p_o' and T_i are not always measured at identical positions from the wall, both sets of data are taken at sufficiently close intervals so that the temperatures corresponding to impact pressure readings at a particular position can be interpolated from a curve faired through the temperature data.

12. The numerical evaluation of the data is done on the NOL Card-Programmed Calculator. The Rayleigh formula is used to compute the Mach number profile from p_o' and p (reference (i)). To evaluate the stagnation temperature, T_o', from the measured T_i values requires reference to the calibration curve of the probe (reference (h)). This curve gives the recovery factor of the probe in terms of the measured total temperature and the pressure, p_2, behind the bow shock in front of the probe

$$r_p = f(p_2/RT_i^{7/4}) \tag{1}$$

13. To calculate the friction velocity, u_τ, for the u^+, y^+ representation (reference (j)) of the boundary layer velocity profiles, the wall shear stress, τ_w, is calculated either from the slope of the velocity profile in the laminar sublayer

$$\tau_w = \left(\mu \frac{du}{dy}\right)_w \tag{2}$$

or from the temperature measurements in the nozzle wall, using the following equations:

$$St_\infty = \frac{(\Delta T/\Delta y)k}{(T_0 - T_w)\, c_p\, \rho_\infty\, u_\infty} \tag{3}$$

and the Reynolds analogy (reference (k))

$$\tau_w = St_\infty \; Pr^{2/3} \; \rho_\infty \; u_\infty^2 \qquad (4)$$

Values of $\Delta T/\Delta y$ are obtained from the measured wall temperature gradient and values of T_e were calculated using $r = Pr^{1/3}$ with $Pr = 0.72$.

RESULTS

Boundary Layer Profiles

14. Naturally turbulent boundary layers were surveyed at free-stream Mach numbers of 5.0 to 8.2. These surveys were made at different Reynolds numbers Re_θ and various rates of heat transfer to the nozzle wall, as listed in the following table:

M_∞	Re_θ	$(T_e - T_w)/T_e$
4.93	5,350	0
5.01	6,480	0.223
5.03	7,950	0.373
5.06	7,370	0.420
5.75	11,600	0.108
5.79	12,400	0.239
5.82	11,400	0.379
6.83	8,550	0.325
6.83	12,640	0.443
6.78	8,400	0.437
6.78	7,900	0.500
7.67	8,130	0.487
8.18	9,540	0.496

A tabulation of the complete data is given in Table I (page 22) and Appendix A. Typical plots of the basic data are shown in Figures 3 through 6. The data points close to the wall that were influenced by the presence of the wall were omitted from all figures and tables.

15. For most of the curves, a dimensional distance has been selected for the abscissa in order to show more clearly the physical differences between the profiles at different heat transfer rates. For the same reason some of the curves and data points have been omitted from Figures 3 through 6. Shape differences are pronounced only in the temperature profiles of the boundary layer, Figures 4 and 5. The static temperature profiles, Figure 5, obtained with heat transfer have a temperature maximum close to the wall. The temperature at the maximum point or those still closer to the wall could not be evaluated from measured air temperatures because of the physical size of the temperature probes. In the cases where heat transfer data have been measured in the nozzle wall (see Table I), the slope of the temperature curve immediately at the wall has been deduced from the temperature gradient in the nozzle wall

$$\left(k\frac{\Delta T}{\Delta y}\right)_{wall} = \left(k\frac{\Delta T}{\Delta y}\right)_{air} \qquad (5)$$

(Values of the thermal conductivity of air have been taken from reference (a)). The curve through the measured data and the computed slope have been joined to give a smooth shape to the static temperature curves. (Since only the square root of the temperature enters into the computation of the velocity, the velocity profile close to the wall was found to be insensitive to errors in T due to incorrect interpolation between the last measured air temperature and the wall temperature.)

16. The velocity profiles at any one Mach number, Figure 6, are similar in the turbulent outer part. A sharp change in slope, near the wall, roughly specifies the extent of the laminar sublayer. Within this sublayer the velocity varies linearly with distance; the slope, however, increases with increasing heat transfer.

17. It should be noted here that velocities deduced from Pitot measurements in the laminar sublayer may be slightly high due to the effect of velocity fluctuations on the Pitot pressure readings close to the wall. Since the fluctuating velocity component, $\overline{u'^2}$ is always positive, the Pitot tube measures total pressures that are always somewhat greater than the effective total pressure by the amount $\frac{1}{2}\rho\overline{u'^2}$. In Figure 7 the variation of $(\overline{u'^2}/u^2)^{\frac{1}{2}}$ with nondimensional distance, y^+, from wall is shown for the incompressible data of references (m), (n), and (o). Although there is considerable scatter, the curve was drawn by giving the greatest consideration to the trend indicated by the larger bulk of data. On the assumption that the incompressible results of

Figure 7 are applicable to the present data, the laminar sublayer velocity profile data can be adjusted by the method given in reference (m). This adjustment indicates that the measured velocities at the edge of the laminar sublayer may be higher than the true velocity by a maximum amount of 3 percent

Nondimensional Velocity Profile Representation

18. Turbulent boundary layer velocity profiles are very often presented in nondimensional coordinates which may be computed either on the basis of wall properties, u^+ and y^+, or local properties at each point in the boundary layer, u^* and y^* (see list of symbols). Figures 8 to 11 show all the measured velocity profiles in the u^+, y^+ coordinate system. A pronounced upward shift of the turbulent portion of the curves with increasing heat transfer is apparent for each Mach number. A similar shift has been observed by Deissler (reference (p)) in his experiments with subsonic compressible turbulent boundary layers in pipes. The position of the three upper curves of Figure 10 relative to each other indicates that a Reynolds number effect is probably superimposed. According to the respective values of the heat transfer parameters for these surveys, a different spacing in the turbulent portion would be expected.

19. In addition to this Reynolds number effect the data in the outer turbulent portion of the profiles (Figures 8 to 11) apparently disperse with Mach number and heat transfer parameter, or some combination thereof. In an effort to determine a parameter which would eliminate the dispersing effect of at least one of the quantities mentioned above, the values of u^* and y^* were evaluated for each point in the boundary layer for each of the measured profiles. A plot of these results indicated a tendency toward a single curve for each Mach number, with the dispersing effect of the different heat transfer rates removed, but not that of the Reynolds number. It was found that this dispersion of the data could be removed by dividing the y^* coordinate by the respective values of the shape parameter (H). The data for any one Mach number then converge to a single curve, (Figure 12). With increasing Mach number the curves fan out in an upward direction. That this displacement is systematic is demonstrated in Figure 13 which shows a cross plot of the data of Figure 12. The naturally turbulent boundary layer data of reference (t), as well as the $M = 0$ results are included in Figure 12.

20. The data of Figures 8 to 11 may be used to examine some of the fundamental assumptions of several of the theoretical treatments of compressible turbulent boundary layers. It is implied in these analyses (references (q), (r), (s) that the

edge of the laminar sublayer occurs at a fixed value of $u^+ = y^+$, and that the slope of the turbulent portion of the u^+, y^+ curve is constant, regardless of Mach number or heat transfer conditions. It should be noted that the results of Figures 8 to 11 show that these assumptions are not generally valid.

Velocity and Thermal Sublayers

21. It is apparent from the curves of Figures 8 through 11 that the u^+, y^+ velocity profile representation only roughly specifies the extent of the laminar sublayer. The edge of the velocity sublayer can be accurately determined from a plot of the coordinates u/u_∞ against y/δ on logarithmic paper. On such a plot it is found that the outer turbulent position of the boundary layer may be well fitted with a straight line, the slope of which is the exponent in the power profile representation of the turbulent boundary layer profiles

$$\frac{u}{u_\infty} = (y/\delta)^{1/n} \qquad (6)$$

In the laminar sublayer, a straight line of unit slope may be drawn quite accurately through the data. The point of intersection of these two straight lines is defined as the edge of the laminar sublayer. Figure 14 demonstrates the results of this procedure applied to the data of several typical profiles. The intersection points indicated are fairly insensitive to the slope of the line faired through the experimental data in the turbulent portion of the velocity profile, and therefore the scatter of the experimental data does not seriously affect the determination of this point. A similar procedure may be used to determine the edge of the thermal sublayer. The thicknesses of the velocity and thermal sublayers have been determined for all of the measured profiles and the values of u_L/u_∞, $(\delta_L/\delta)_u$, $(\delta_L/\delta)_T$, and n are tabulated in Table I (page 22).

22. A comparison between the values of $(\delta_L/\delta)_u$ and $(\delta_L/\delta)_T$, Table I, shows that the thermal sublayer is in all cases thicker than the velocity sublayer. According to the analysis of reference (v) the relative thicknesses of the thermal and velocity sublayers are related to the turbulent Prandtl number. For the present case of thermal sublayers thicker than the velocity sublayer Reichardt's theory predicts a turbulent Prandtl number larger than the molecular Prandtl number. Preliminary evaluation of this quantity for

the zero heat transfer case of $M = 4.93$ and a molecular Prandtl number of 0.72 using the equations given by Rubesin (reference (w)) yielded a value for the turbulent Prandtl number of the order of 0.9.

Discussion of Skin Friction Data

23. Because many of the theoretical treatments of compressible turbulent boundary layers involve properties of the laminar sublayer, emphasis was placed on determining the velocity and temperature distributions in this region. Furthermore these data facilitate the accurate determination of surface shear stress from the velocity profile slope near the wall.

24. For most of the measured profiles, the surface shear stress was calculated from the slope of the velocity profile in the laminar sublayer and the heat transfer data using Reynolds analogy, as described previously. Values of c_f and St_∞ obtained for all the profiles are tabulated in Table I. In general the values of c_f determined from the velocity profile data are up to 5 percent larger than those determined from the heat transfer measurements. A possible explanation for this discrepancy may be given by considering the previously mentioned effect of the velocity fluctuations on the Pitot pressure data. Assuming that the incompressible results of Figure 7 can be applied, the laminar sublayer velocity profile data were corrected by the method indicated in reference (m). Values of wall shear stress were then computed from the adjusted velocity profiles. This procedure brings the shear stress values from the heat transfer data and velocity profile data in closer agreement (see Table I). The two values are well within the experimental accuracy of the data.

25. The good agreement between skin friction coefficients obtained from the velocity profile data and those determined from the measured heat transfer, using Reynolds analogy demonstrates the applicability of Reynolds analogy at hypersonic Mach numbers. That the Reynolds analogy is applicable for supersonic flow up to a Mach number of about 3.2 has been shown by Seiff (reference (x)). The present data, plotted together with those of reference (x), show that at hypersonic Mach numbers the Reynolds analogy maintains the same form found to be accurate for lower supersonic speeds. The present data are especially convincing evidence because the Stanton number and the skin friction coefficient were determined simultaneously by two independent experimental methods whereas the results of reference (x) were calculated by "interpolating the skin friction data to equal conditions of Mach number, wall to free stream temperature ratio, and Reynolds number."

26. In the figures which follow, the experimental values of c_f used are those determined by the velocity-profile slope technique. These values of c_f were used, not in preference to those obtained from the heat transfer measurements, but only because there are some cases for which heat transfer measurements are not available and it was desired to preserve consistency in the plotted results.

27. The values of c_{fi} used to form the ratio c_f/c_{fi} were calculated from the Karman-Schoenherr equation for the same Re_θ value for zero heat transfer

$$c_{fi} = \frac{0.586}{(\log_{10}2\ Re_\theta)(\log_{10}2\ Re_\theta + 0.868)} \qquad (7)$$

The Reynolds number based on momentum thickness was used instead of the customary Reynolds number based on the distance from the leading edge. A Reynolds number based on a boundary layer parameter was selected because of the arbitrariness inherent in calculating an effective leading edge for boundary layer measurements on a wind tunnel wall.

28. The variation of c_f/c_{fi} with heat transfer parameter $(T_e - T_w)T_e$ is shown in Figure 15 for all of the data of the present investigation. Also shown on this figure are curves calculated using an extended Donaldson analysis reported in reference (u). For those values of Mach number for which several data points are available (M = 5.0, 5.8, and 6.8), the results indicate that increasing values of heat transfer parameter have little effect on the skin friction ratio. On the other hand, Van Driest and Monaghan (references (s), (y)) predict an increase in the skin friction ratio up to about 10 percent for the highest heat transfer case investigated in the present experiments. It should be noted, however, that it is implied in these analyses that the edge of the laminar sublayer occurs at fixed values of u^+ and y^+, and the slope of the turbulent portion of the u^+, y^+ curve remains constant regardless of Mach number or heat transfer conditions. As pointed out previously, the results given in Table I show that these assumptions are not generally valid. This is more evident from Figure 16 in which the values of $u_L^+ = y_L^+$ are plotted as a function of the heat transfer parameter. Also shown are the associated theoretical curves derived from reference (u). These figures

indicate that Mach number has little influence on the variation of $u_L^+ = y_L^+$ with $(T_e - T_w)/T_e$. It appears, however, from these results that caution should be exercised in using theories which embody constant values of $u_L^+ = y_L^+$ for cases of heat transfer.

29. The variation of c_f/c_{fi} with Mach number is shown in Figure 17 together with the direct skin friction measurements of Coles (reference (z)) and the deduced skin friction data of references (a), (q), (r), (t), (y), (z), and (aa). In the preparation of this figure the data for $M = 5$ and 6.8 were reduced to the case of zero heat transfer by fitting the results of Figure 15 with a straight line using the method of least squares. For the other Mach numbers the zero heat transfer points were obtained by estimating the slope of a straight line through the data consistent with the $M = 5$ and 6.8 results. The position of the data points on this figure was fixed by plotting the variation of c_f/c_{fi} against Re_θ for each Mach number and selecting the values of c_f/c_{fi} at a constant value of Re_θ of 8,000. This value of Re_θ was selected because it represented a Reynolds number for which the greatest overlap of data existed. It is apparent that the c_f/c_{fi} variation with Mach number is a smooth continuous curve for a constant Reynolds number. Also shown in this figure are the theoretical predictions of references (q) and (u) for a constant Reynolds number of 8,000 and zero heat transfer. The close fit of the experimental data with the theoretical curves indicates that the theories of references (q) and (u) may be used to predict with good accuracy the variation of skin friction coefficients with Mach number for the zero heat transfer case.

CONCLUDING REMARKS

30. Detailed investigations of turbulent boundary layer velocity and temperature profiles have been made on a nozzle wall of the NOL 12 x 12 cm Hypersonic Tunnel No. 4 at Mach numbers of 5.0, 5.8, 6.8, 7.7, and 8.2 for varying rates of surface heat transfer.

31. The experimental results show that turbulent boundary layer profiles in hypersonic flow qualitatively resemble turbulent boundary layer profiles in incompressible flow in many details.

32. All velocity profiles measured can be fitted with a power law in the outer turbulent portion.

33. As in the case of incompressible flow, the turbulent portion of the profiles differs in shape from the logarithmic-law velocity profile. The discrepancy increases with increasing heat transfer.

34. The dispersing effects of Reynolds number and heat transfer parameter exhibited in the u^+, y^+ velocity profile representation for the outer turbulent portion could be removed by basing the coordinates on local properties at each point in the boundary layer and dividing the distance parameter by the respective shape parameter (II). The data for any one Mach number then fall on a single curve. The velocity profile curves show a systematic displacement with Mach number.

35. The velocity profiles in the laminar sublayer are linear. The ratio of laminar sublayer thickness to total boundary layer thickness $(\delta_L/\delta)_u$ decreases slightly with increasing heat transfer rate but increases considerably with increasing Mach number at the same heat transfer rates.

36. The $u^+ = y^+$ value at the edge of the laminar sublayer for the zero heat transfer case is close to the incompressible flow value. However, this $u^+ = y^+$ value is found to increase with increasing heat transfer for any given Mach number.

37. The ratio of the thermal sublayer thickness to the total boundary layer thickness $(\delta_L/\delta)_T$ was found larger than $(\delta_L/\delta)_u$. The thermal sublayer thickness ratio is unaffected by heat transfer but somewhat affected by Reynolds number.

38. The data strongly support the applicability of Reynolds analogy for turbulent boundary layers in hypersonic flow.

39. Values of skin friction coefficients calculated from the heat transfer measurements by using Reynolds analogy agree to within 5 percent with those skin friction values deduced from the velocity profile slope in the laminar sublayer.

40. For the test range of the heat transfer parameter $(T_e - T_w)/T_e$ (approximately 0 to 0.5), values of the skin friction coefficient are found to be only slightly affected by heat transfer rate and are in accord with the direct skin friction measurements of Coles and other investigators when the results are based on a single value of Reynolds number.

41. The present results extend the range of available skin friction and heat transfer data to a Mach number of 8.2.

42. The detailed measurements of velocity and temperature distributions across turbulent boundary layers in hypersonic flow presented here enlarge the fund of available data for turbulent boundary layers in compressible flows.

REFERENCES

(a) Chapman, Dean R., and Kester, Robert H., "Measurements of Turbulent Skin Friction on Cylinders in Axial Flow at Subsonic and Supersonic Velocities," paper presented at the 21st Annual Meeting, I.A.S., New York, January 26-29, 1953 (Preprint No. 391).

(b) Wegener, P., "Summary of Recent Experimental Investigations in the NOL Hyperballistics Wind Tunnel," Journal of the Aeronautical Sciences, Vol. 18, No. 10, p. 665, October 1951.

(c) Wegener, Peter P., and Lobb, Kenneth R., "An Experimental Study of Hypersonic Wind-Tunnel Diffuser," Journal of the Aeronautical Sciences, Vol. 20, No. 2, p. 105, February 1953.

(d) Wegener, Peter P.; Lobb, R. K.; Winkler, E. M.; Sibulkin, M.; and Staab, H., "NOL Hypersonic Tunnel No. 4 Results V: Experimental and Theoretical Investigation of a Cooled Hypersonic Wedge Nozzle," NAVORD Report 2701, April, 1953.

(e) Wegener, Peter P.; Winkler, E. M.; and Sibulkin, M., "A Measurement of Turbulent Boundary Layer Profiles and Heat Transfer Coefficient at M = 7," Journal of the Aeronautical Sciences, Vol. 20, No. 3, p. 221, March 1953.

(f) Tsien, H., "Superaerodynamics - The Mechanics of Rarefied Gases," Journal of the Aeronautical Sciences, Vol. 13, No. 12, December 1946.

(g) Kane, E. D., and Maslach, G. J., "Impact-Pressure Interpretation in a Rarefied Gas at Supersonic Speeds," NACA TN 2210, October 1950.

(h) Winkler, E. M., "Stagnation Temperature Probes for Use at High Supersonic Speeds and Elevated Temperatures," NAVORD Report 3834.

(i) Liepmann, H. W., and Puckett, A. E., "Introduction to Aerodynamics of a Compressible Fluid," GALCIT Aeronautical Series, John Wiley and Sons, Inc., New York, 1947.

(j) von Karman, Th., "Turbulence and Skin Friction," Journal of the Aeronautical Sciences, Vol. 1, No. 1, January 1934.

(k) Johnson, H. A., and Rubesin, M. W., "Aerodynamic Heating and Convective Heat Transfer - Summary of Literature Survey," Presented at the Annual Meeting of the American

Society of Mechanical Engineers, New York, November 28-December 3, 1948.

(l) Eckert, E.R.G., "Introduction to the Transfer of Heat and Mass," McGraw - Hill, New York, 1950.

(m) Laufer, John, "The Structure of Turbulence in Fully Developed Pipe Flow," NACA TN 2954.

(n) Laufer, John, "Investigation of Turbulent Flow in a Two-Dimensional Channel," NACA TN 1053.

(o) Little, Barney H., and Wibur, Stafford W., "Turbulence Intensity Measurements in a Jet of Air Issuing from a Long Tube," NACA TN 2361.

(p) Deissler, R. G., and Eian, C. S., "Analytical and Experimental Investigation of Fully Developed Turbulent Flow of Air in a Smooth Tube with Heat Transfer with Variable Fluid Properties," NACA TN 2629, February, 1952.

(q) Wilson, R. E., "Turbulent Boundary Layer Characteristics at Supersonic Speeds - Theory and Experiment," Journal of the Aeronautical Sciences, Vol. 17, No. 9, September 1950.

(r) Rubesin, Morris, W.; Maydew, Randall C.; and Varga, Steven A., "An Analytical and Experimental Investigation of the Turbulent Boundary Layer on a Flat Plate at Supersonic Speeds," NACA TN 2305, 1951.

(s) Van Driest, E. R., "The Turbulent Boundary Layer for Compressible Fluids on a Flat Plate with Heat Transfer," North American Aviation Rep. AL - 1006, February 20, 1950.

(t) Brinich, Paul F., and Diaconis, Nick S.,"Boundary Layer Development and Skin Friction at Mach Number of 3.05," NACA TN 2742, 1952.

(u) Persh, Jerome, "A Theoretical Investigation of Turbulent Boundary Layer Flow with Heat Transfer at Supersonic and Hypersonic Speeds," NAVORD Report 3854, to be published.

(v) Reichardt, H., "Der Einfluss der wandnahen Stroemung auf den turbulenten Waermeuebergang," Mitteilungen aus dem Max-Planck-Institut fuer Stroemungsforschung, No. 3, 1950.

(w) Rubesin, Morris W., "A Modified Reynolds Analogy for the Compressible Turbulent Boundary Layer on a Flat Plate," NACA TN 2917, 1953.

(x) Seiff, A., "Examination of the Existing Data on the Heat Transfer of Turbulent Boundary Layers at Supersonic

Speeds from the Viewpoint of Reynolds Analogy, NACA TN 3284, August 1954.

(y) Monaghan, R. J., "Comparison Between Experimental Measurements and Suggested Formula for the Variation of Turbulent Skin Friction in Compressible Flow," British ARC C.P. No. 45 (13260), 1951.

(z) Coles, Donald, "Measurements in the Boundary Layer on a Smooth Flat Plate in Supersonic Flow," Thesis, California Institute of Technology, May 1953.

(aa) Monaghan, R. J. and Cooke, J. R., 'The Measurement of Heat Transfer and Skin Friction at Supersonic Speeds, Part IV," British ARC C.P. No. 140 (15,400), 1953.

(bb) Monaghan, R. J. and Cooke, J. R., 'The Measurement of Heat Transfer and Skin Friction at Supersonic Speeds, Part III,' British RAE Technical Note No. AERO 2129, 1954.

(cc) Korkegi, R. H., 'Transition Studies and Skin Friction Measurements on an Insulated Flat Plate at a Hypersonic Mach Number," GALCIT Memorandum No. 17, 1954.

M_∞ = 4.93 p_o = 3.08 atm
Re_θ = 5,350 T_o = 325.4° K
$\frac{Te - T_w}{Te}$ = 0 T_∞ = 55.5° K
u_∞ = 736.4 m/sec
$\frac{T_w}{T_\infty}$ = 5.42

y (mm)	M	T/T_∞	u/u_∞
20.02	4.93	1.000	1.000
19.38	4.93	1.000	1.000
18.75	4.92	1.005	1.000
18.11	4.90	1.010	.999
17.48	4.87	1.023	.998
16.21	4.78	1.055	.995
14.94	4.65	1.104	.990
13.67	4.47	1.175	.982
12.40	4.27	1.262	.972
11.13	4.06	1.360	.959
9.85	3.85	1.480	.949
8.58	3.61	1.610	.929
7.31	3.36	1.776	.908
6.66	3.24	1.860	.896
6.05	3.10	1.970	.884
5.41	2.97	2.080	.868
4.77	2.84	2.195	.854
4.14	2.70	2.330	.835
3.51	2.55	2.488	.814
2.87	2.41	2.640	.794
2.24	2.27	2.800	.771
1.73	2.14	2.950	.746
1.22	1.92	3.235	.700
.96	1.75	3.470	.662
.71	1.47	3.890	.588
.55	1.26	4.210	.524
.47	1.05	4.520	.453
.33	.80	4.750	.357
.24	.62	5.060	.283

M_∞ = 5.01 p_o = 5.01 atm
Re_θ = 6,480 T_o = 398.7° K
$\frac{Te - T_w}{Te}$ = .224 T_∞ = 66.2° K
u_∞ = 817.7 m/sec
$\frac{T_w}{T_\infty}$ = 4.29

y (mm)	M	T/T_∞	u/u_∞
19.56	5.01	1.000	1.000
17.65	4.99	1.007	.999
17.02	4.97	1.012	.999
15.75	4.91	1.034	.997
14.48	4.79	1.072	.990
9.40	4.02	1.375	.941
4.32	2.89	2.045	.823
1.78	2.29	2.533	.726
1.40	2.17	2.640	.706
1.14	2.07	2.740	.684
.89	1.90	2.940	.649
.63	1.60	3.283	.580
.53	1.44	3.490	.537
.48	1.37	3.525	.515
.43	1.22	3.725	.469
.38	1.11	3.800	.432
.33	1.01	3.903	.398
.30	.95	3.950	.377
.28	.88	4.000	.353
.25	.80	4.060	.322
.23	.72	4.125	.292
.18	.71	4.225	.230

APPENDIX A

M_∞ = 5.03 p_o = 7.85 atm
Re_θ = 7,950 T_o = 513° K
$\frac{T_e - T_w}{T_e}$ = .374 T_∞ = 84.6° K
u_∞ = 927.8 m/sec
$\frac{T_w}{T_\infty}$ = 3.49

y (mm)	M	T/T_∞	u/u_∞
18.60	5.03	1.000	1.000
17.33	5.02	1.010	.998
14.53	4.94	1.022	.993
13.52	4.83	1.052	.985
8.43	3.93	1.379	.917
3.35	2.76	2.015	.780
2.72	2.59	2.133	.753
2.08	2.45	2.220	.725
1.83	2.40	2.250	.716
.57	2.33	2.296	.702
1.45	2.32	2.300	.702
1.32	2.27	2.340	.691
1.19	2.24	2.353	.683
1.07	2.18	2.405	.674
.94	2.13	2.445	.663
.81	2.02	2.490	.634
.69	1.92	2.640	.620
.56	1.75	2.820	.584
.43	1.53	3.060	.532
.30	1.24	3.195	.441
.30	1.20	3.240	.430
.18	.70	3.505	.261

M_∞ = 5.06 p_o = 8.58 atm
Re_θ = 7,370 T_o = 562° K
$\frac{T_e - T_w}{T_e}$ = .420 T_∞ = 91.5° K
u_∞ = 971.8 m/sec
$\frac{T_w}{T_\infty}$ = 3.27

y (mm)	M	T/T_∞	u/u_∞
21.72	5.06	1.000	1.000
19.18	5.06	1.004	1.000
14.10	4.86	1.058	.987
9.02	4.14	1.295	.930
3.94	3.01	1.830	.804
2.67	2.68	2.023	.752
2.03	2.52	2.120	.724
1.65	2.43	2.175	.707
1.42	2.38	2.200	.696
1.40	2.37	2.208	.696
1.17	2.30	2.250	.681
1.04	2.24	2.295	.670
.91	2.17	2.347	.656
.79	2.06	2.440	.635
.76	2.05	2.440	.633
.66	1.94	2.540	.610
.53	1.75	2.725	.570
.47	1.62	2.840	.539
.41	1.52	2.815	.504
.28	1.16	3.030	.400

APPENDIX A

M_∞ = 5.75 p_o = 13.4 atm
Re_θ = 11,600 T_o = 401° K
$\frac{Te - T_w}{Te}$ = .108 T_∞ = 52.7° K
u_∞ = 836 m/sec
$\frac{T_w}{T_\infty}$ = 6.19

y (mm)	M	T/T_∞	u/u_∞
19.90	5.75	1.000	1.000
18.40	5.72	1.005	.999
17.40	5.66	1.023	.997
16.10	5.55	1.060	.994
14.86	5.33	1.133	.988
12.32	4.77	1.354	.968
11.05	4.47	1.500	.953
9.79	4.15	1.673	.935
8.54	3.86	1.855	.914
7.27	3.53	2.080	.887
6.00	3.22	2.320	.855
4.73	2.92	2.593	.818
3.46	2.63	2.875	.777
2.82	2.45	3.080	.748
2.18	2.29	3.260	.721
1.81	2.23	3.338	.708
1.68	2.18	3.400	.698
1.55	2.14	3.440	.692
1.17	2.03	3.590	.669
.99	1.91	3.760	.646
.79	1.76	3.970	.611
.66	1.63	4.160	.578
.61	1.56	4.260	.562
.53	1.45	4.450	.532
.41	1.22	4.810	.465
.35	1.08	5.020	.420
.28	.93	5.110	.371

M_∞ = 5.79 p_o = 16.75 atm
Re_θ = 12,400 T_o = 477° K
$\frac{Te - T_w}{Te}$ = .238 T_∞ = 61.9° K
u_∞ = 914 m/sec
$\frac{T_w}{T_\infty}$ = 5.35

y (mm)	M	T/T_∞	u/u_∞
22.53	5.79	1.000	1.000
20.00	5.75	1.013	.999
18.74	5.74	1.016	.999
17.46	5.67	1.039	.997
16.20	5.53	1.081	.993
13.70	5.12	1.215	.975
11.11	4.60	1.415	.946
8.60	4.04	1.692	.907
6.04	3.43	2.075	.853
4.25	2.99	2.418	.803
3.74	2.86	2.525	.787
3.50	2.81	2.580	.778
2.73	2.60	2.780	.748
2.23	2.45	2.923	.725
1.97	2.40	2.970	.715
1.46	2.29	3.090	.694
1.21	2.18	3.220	.677
.95	2.09	3.295	.657
.70	1.87	3.550	.608
.57	1.70	3.740	.568
.45	1.46	4.000	.507
.33	1.14	4.390	.411
.21	.76	4.780	.286

APPENDIX A

M_∞ = 5.82 p_o = 16.95 atm
Re_θ = 11,400 T_o = 551° K
$\frac{T_e - T_w}{T_e}$ = .379 T_∞ = 70.9° K
u_∞ = 982 m/sec
$\frac{T_w}{T_\infty}$ = 4.41

y (mm)	M	T/T_∞	u/u_∞
22.40	5.82	1.000	1.000
21.90	5.82	1.000	1.000
19.30	5.82	1.000	.999
18.10	5.76	1.018	.996
16.80	5.70	1.028	.992
14.30	5.37	1.120	.975
11.75	4.88	1.280	.948
9.20	4.33	1.505	.911
7.94	4.03	1.645	.888
6.65	3.75	1.795	.862
5.40	3.37	2.040	.827
4.12	3.05	2.273	.789
3.48	2.86	2.420	.765
2.84	2.70	2.560	.742
1.48	2.31	2.920	.679
1.07	2.21	3.015	.658
.81	2.04	3.260	.633
.56	1.74	3.540	.562
.43	1.36	3.980	.466
.31	1.08	4.180	.380
.13	.74	4.600	.261

M_∞ = 6.83 p_o = 15.3 atm
Re_θ = 8,550 T_o = 467.6° K
$\frac{T_e - T_w}{T_e}$ = .326 T_∞ = 45.3° K
u_∞ = 920.3 m/sec
$\frac{T_w}{T_\infty}$ = 6.34

y (mm)	M	T/T_∞	u/u_∞
23.80	6.83	1.000	1.000
22.53	6.81	1.000	1.000
21.26	6.74	1.010	1.000
20.62	6.66	1.033	.997
19.99	6.56	1.059	.992
18.72	6.31	1.129	.987
16.18	5.70	1.327	.966
13.64	5.05	1.595	.940
11.10	4.43	1.932	.907
8.56	3.84	2.343	.866
6.02	3.26	2.859	.812
3.48	2.67	3.544	.740
2.21	2.36	3.960	.693
1.42	2.01	4.564	.633
1.17	1.17	5.010	.584
.94	1.47	5.612	.516
.91	1.48	5.580	.515
.79	1.25	6.052	.453
.71	1.10	6.337	.407
.66	1.02	6.463	.388
.61	.95	6.588	.360
.56	.86	6.717	.328
.51	.78	6.735	.299
.41	.63	6.902	.244

APPENDIX A

M_∞ = 6.78 p_o = 21.1 atm
Re_θ = 8,400 T_o = 586° K
$\frac{Te - T_w}{Te}$ = .438 T_∞ = 57.5° K
u_∞ = 1031 m/sec
$\frac{T_w}{T_\infty}$ = 5.22

y (mm)	M	T/T_∞	u/u_∞
22.04	6.78	1.000	1.000
20.88	6.68	1.006	.996
18.34	6.29	1.112	.986
17.07	6.03	1.188	.977
15.80	5.71	1.301	.968
14.53	5.39	1.417	.954
13.26	5.06	1.554	.938
11.99	4.74	1.701	.919
10.72	4.43	1.864	.899
9.45	4.14	2.030	.877
8.18	3.84	2.223	.852
6.91	3.56	2.428	.825
5.74	3.29	2.651	.796
5.64	3.29	2.651	.797
4.37	2.97	2.955	.759
3.10	2.67	3.288	.720
1.83	2.37	3.651	.673
1.32	2.19	3.914	.640
1.07	1.94	4.343	.595
.81	1.60	4.988	.522
.68	1.44	5.301	.482
.55	1.17	5.421	.402
.44	.90	5.600	.314
.44	.83	5.545	.323
.31	.76	5.527	.228

M_∞ = 6.83 p_o = 28.5 atm
Re_θ = 12,640 T_o = 586° K
$\frac{Te - T_w}{Te}$ = .444 T_∞ = 56.7° K
u_∞ = 1031.2 m/sec
$\frac{T_w}{T_\infty}$ = 5.24

y (mm)	M	T/T_∞	u/u_∞
25.20	6.83	1.000	1.000
22.66	6.83	1.000	1.000
21.39	6.82	1.000	.999
20.12	6.79	1.005	.997
18.85	6.68	1.025	.987
17.58	6.45	1.079	.981
15.04	5.84	1.251	.956
12.50	5.16	1.505	.927
11.23	4.82	1.658	.909
9.96	4.49	1.830	.890
7.42	3.86	2.215	.841
4.88	3.23	2.710	.779
3.61	2.87	3.073	.737
2.97	2.69	3.260	.713
2.34	2.54	3.420	.687
1.71	2.40	3.560	.664
1.33	2.28	3.690	.641
1.07	2.14	3.750	.608
.82	1.92	4.140	.570
.56	1.52	4.640	.479
.31	.97	5.180	.263
.28	.72	5.210	.240

APPENDIX A

M_∞ = 6.78 p_o = 21.4 atm
Re_θ = 7,960 T_o = 639.2° K
$\frac{Te - T_w}{Te}$ = .499 T_∞ = 62.7° K
u_∞ = 1076.6 m/sec
$\frac{T_w}{T_\infty}$ = 4.64

y (mm)	M	T/T_∞	u/u_∞
20.12	6.78	1.000	1.000
19.48	6.69	1.018	.995
18.85	6.61	1.037	.992
18.21	6.52	1.060	.991
15 67	5.97	1.215	.972
13.13	5.34	1.426	.941
10.59	4.69	1.701	.902
8.05	4.06	2.043	.856
5.51	3.44	2.470	.798
2.97	2.80	3.054	.721
1.70	2.47	3.377	.671
1.45	2.39	3.474	.658
1.22	2.24	3.637	.631
.96	2.00	3.850	.580
.76	1.71	4.078	.509
.71	1.61	4.187	.486
.61	1.40	4.386	.433
.51	1.16	4.608	.367
.43	.98	4.791	.316
.41	.94	4.760	.302
.33	.76	4.850	.246
.30	.70	4.860	.228

M_∞ = 7.67 p_o = 24.2 atm
Re_θ = 8,130 T_o = 645° K
$\frac{Te - T_w}{Te}$ = .488 T_∞ = 50.5° K
u_∞ = 1093 m/sec
$\frac{T_w}{T_\infty}$ = 5.94

y (mm)	M	T/T_∞	u/u_∞
29.16	7.67	1.000	1.000
26.62	7.67	1.000	1.000
24.08	7.57	1.015	.993
21.54	7.03	1.127	.973
19.00	6.32	1.328	.951
16.46	5.62	1.590	.922
13.92	4.94	1.915	.891
12.65	4.60	2.107	.869
11.38	4.34	2.250	.852
10.11	4.03	2.520	.833
8.84	3.78	2.708	.811
7.57	3.52	2.947	.788
6.30	3.28	3.208	.766
5.03	3.03	3.475	.736
3.76	2.74	3.850	.701
2.49	2.42	4.305	.655
1.85	2.11	4.675	.594
1.73	2.03	4.740	.576
1.47	1.87	4.860	.537
1.22	1.60	5.200	.475
.96	1.30	5.565	.399
.77	1.00	5.870	.315
.68	.86	5.870	.271
.46	.55	6.260	.179

APPENDIX A

$M_\infty = 8.18$ $\quad p_o = 31.8$ atm

$Re_\theta = 9{,}540$ $\quad T_o = 655^\circ$ K

$\frac{Te - T_w}{Te} = .495$ $\quad T_\infty = 45.5^\circ$ K

$u_\infty = 1109$ m/sec

$\frac{T_w}{T_\infty} = 6.6$

y (mm)	M	T/T_∞	u/u_∞
26.50	8.18	1.000	1.000
25.30	8.05	1.014	.993
24.00	7.88	1.045	.985
21.50	7.30	1.180	.966
18.90	6.61	1.360	.942
16.40	5.93	1.599	.916
13.80	5.29	1.879	.886
11.30	4.70	2.200	.854
8.80	4.16	2.579	.817
6.22	3.63	3.037	.773
4.95	3.33	3.334	.745
3.73	3.02	3.680	.708
2.50	2.61	4.080	.644
2.21	2.46	4.280	.622
1.65	2.07	4.750	.558
1.45	1.83	4.902	.514
1.30	1.61	5.403	.455
1.00	1.19	5.806	.355

APPENDIX A

TABLE I. TABULATION OF OPERATING CONDITIONS AND DERIVED PARAMETERS FOR ALL MEASURED BOUNDARY LAYER PROFILES

M_∞	p_o, Atm	δ mm	δ^* mm	θ mm	n	Re_θ	Experimental $c_f \times 10^4$ *	Experimental $c_f \times 10^4$ **	$\frac{c_f}{c_{fi}}$ ***	$St_\infty \times 10^4$	$\frac{T_o - T_w}{T_o}$	$\frac{u_L}{u_\infty}$	$\left(\frac{\delta_L}{\delta}\right)_u$	$\left(\frac{\delta_L}{\delta}\right)_T$	$u_L^+ = y_L^+$
4.93	3.68	19	7.12	0.624	7.1	5,350	10.9	--	0.369	--	0	0.655	0.0375	0.0510	11.80
5.01	5.01	18	6.13	0.768	6.9	6,480	10.9	10.6	0.381	6.50	0.224	0.615	0.0280	0.0500	12.90
5.03	7.03	16	5.82	0.815	7.2	7,950	9.43	9.69	0.341	5.96	0.374	0.585	0.0250	0.0475	14.40
5.06	8.58	17	5.72	0.871	6.7	7,370	9.18	--	0.328	--	0.420	0.575	0.0240	0.0485	14.88
5.75	13.40	17.5	8.31	0.643	6.3	11,600	8.70	8.00	0.312	4.97	0.108	0.667	0.0237	0.0422	11.40
5.79	16.75	20	7.89	0.715	6.4	12,400	7.25	7.19	0.282	4.43	0.238	0.580	0.0230	0.0385	13.15
5.82	16.95	19	7.35	0.865	6.5	11,400	7.10	6.92	0.269	4.25	0.379	0.580	0.0263	0.043	14.78
6.83	15.3	23	10.91	0.784	5.8	8,510	6.83	6.66	0.251	4.09	0.326	0.600	0.0450	0.068	13.00
6.78	21.1	22	10.34	0.825	5.6	8,400	6.66	6.65	0.244	4.13	0.438	0.580	0.0370	0.069	13.90
6.83	28.5	21	9.41	0.903	5.8	12,640	5.93	5.82	0.234	3.56	0.444	0.550	0.0312	0.051	14.06
6.78	21.4	20	9.29	0.882	5.9	7,960	6.94	6.70	0.251	4.12	0.499	0.586	0.0400	0.070	14.60
7.67	24.2	26	13.12	1.052	5.5	8,130	5.98	--	0.217	--	0.488	0.600	0.0580	0.090	14.30
8.18	31.3	26.5	13.16	1.140	5.5	9,540	5.30	4.96	0.192	3.06	0.495	0.612	0.0660	0.090	14.62

Note: Unless specified otherwise, all fluid properties involved in the Reynolds numbers and skin friction coefficients are evaluated at the edge of the boundary layer.

* obtained from the velocity profile slope at the wall

** obtained from heat transfer measurements in tunnel wall

*** c_{fi} obtained from Karman-Schoenherr equation for zero heat transfer

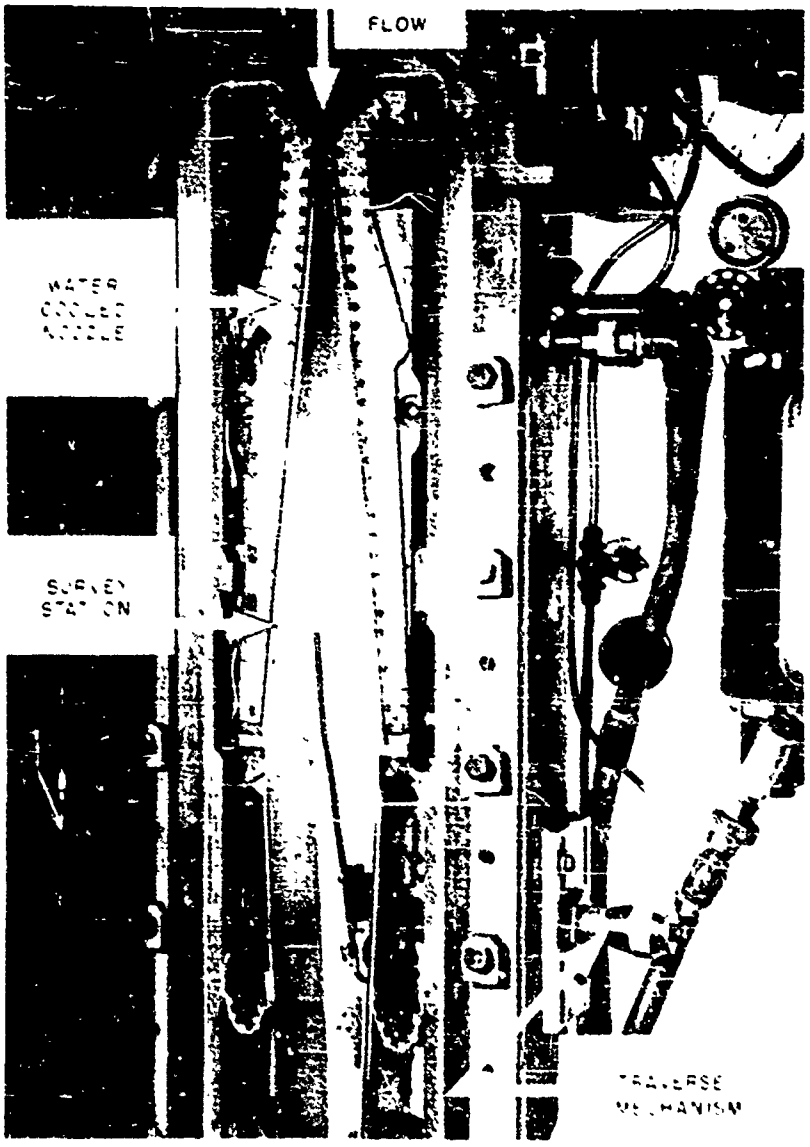

FIG 1 NOL 12 x 12 CM HYPERSONIC TUNNEL

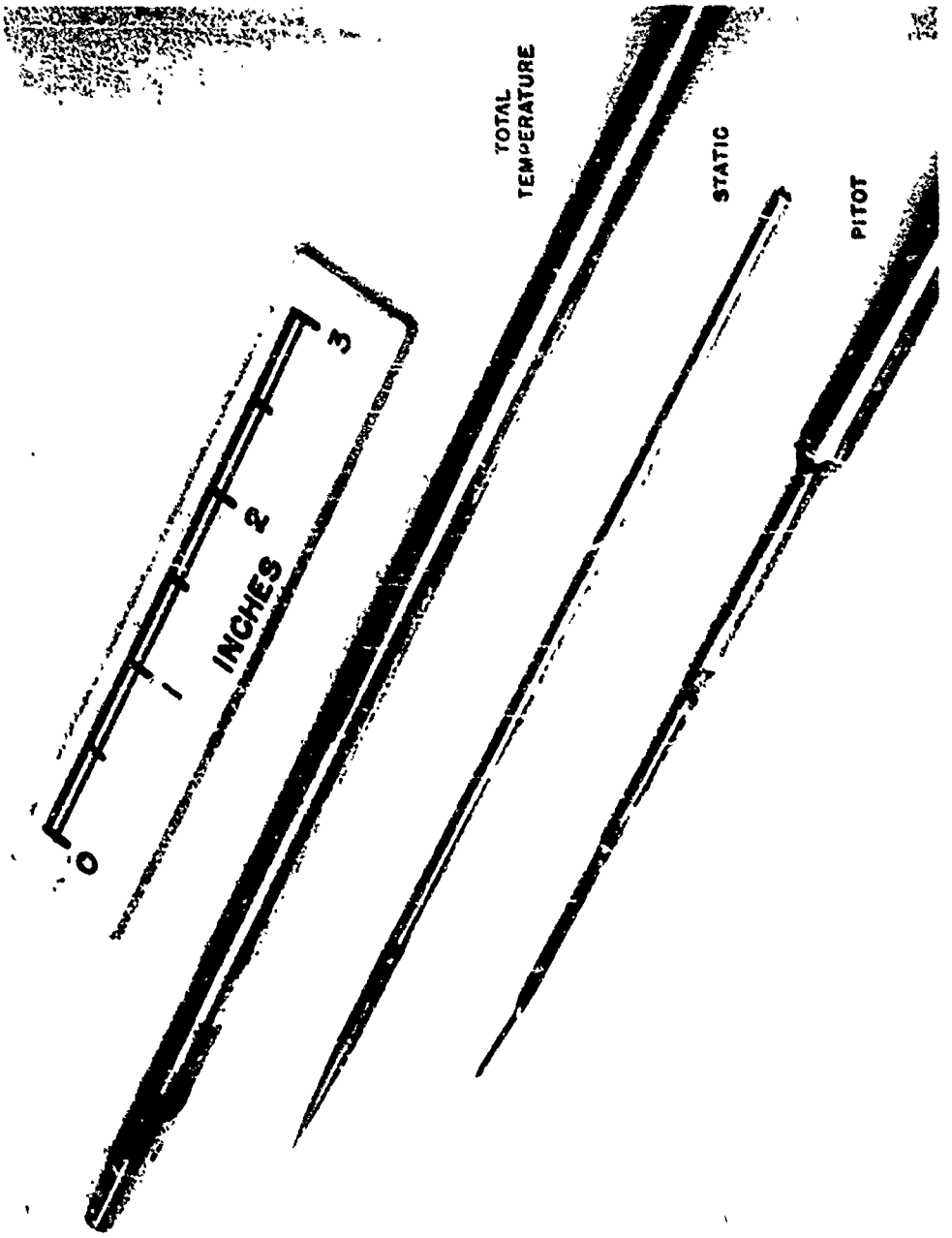

FIG. 2 TEMPERATURE AND PRESSURE PROBES

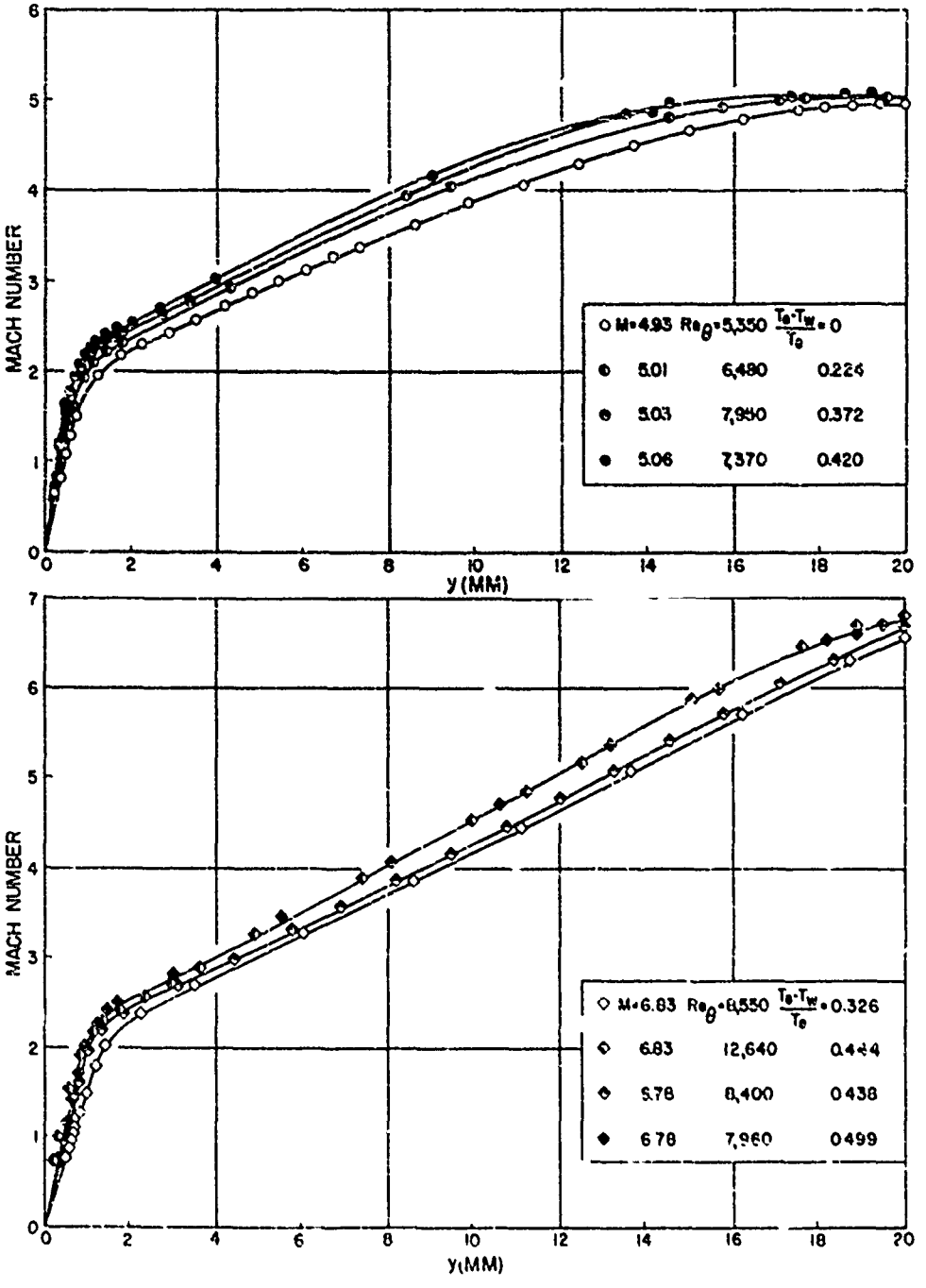

FIG. 3 MACH NUMBER VARIATION ACROSS BOUNDARY LAYER FOR FREE-STREAM MACH NUMBERS OF 5 AND 6.8 AND VARIOUS RATES OF HEAT TRANSFER

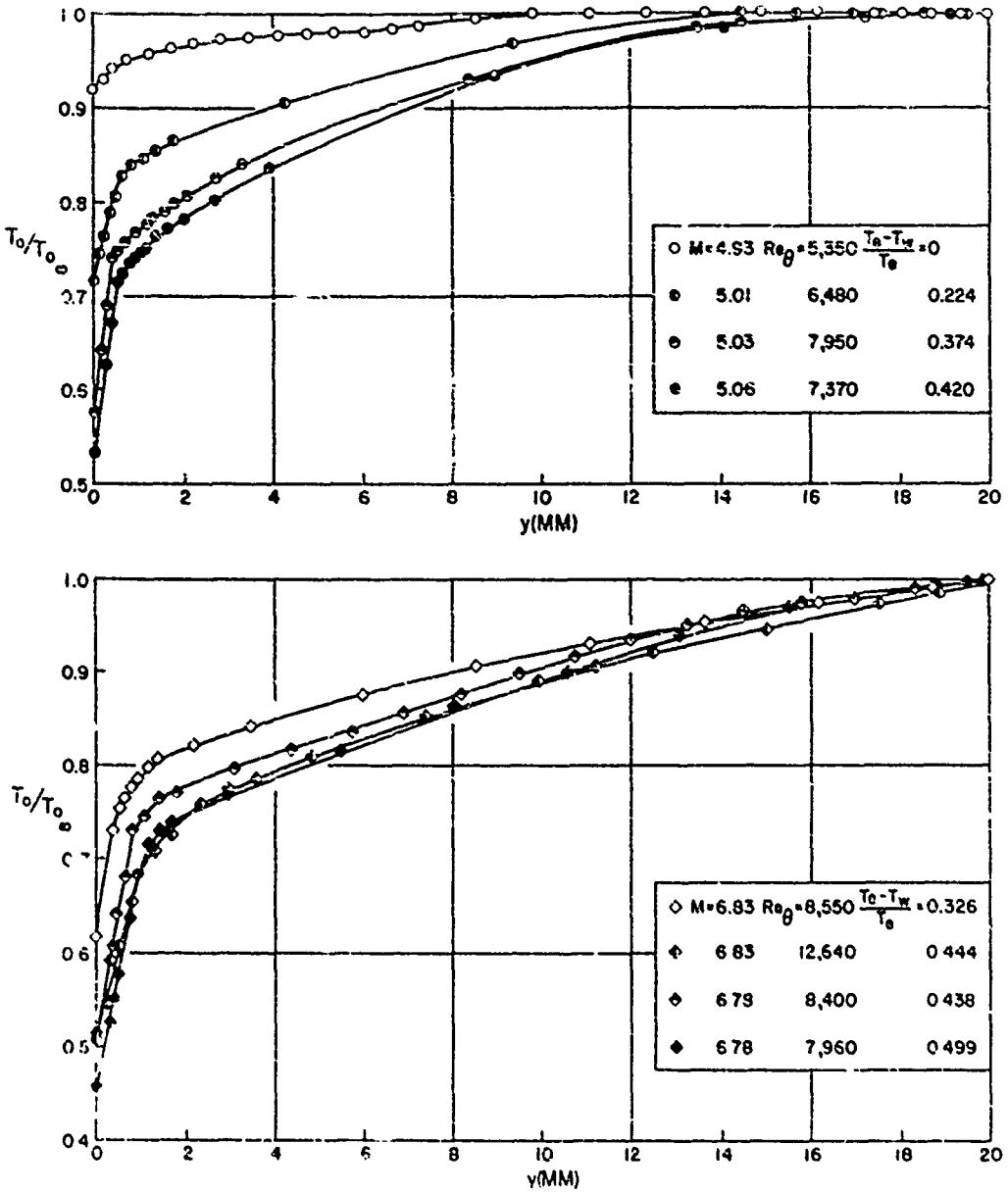

FIG. 4 STAGNATION TEMPERATURE VARIATION ACROSS BOUNDARY LAYER FOR FREE-STREAM MACH NUMBERS OF 5 AND 6.8 AND VARIOUS RATES OF HEAT TRANSFER

VALUES BETWEEN $0<y<0.5$ BASED ON INTERPOLATED T_t VALUES

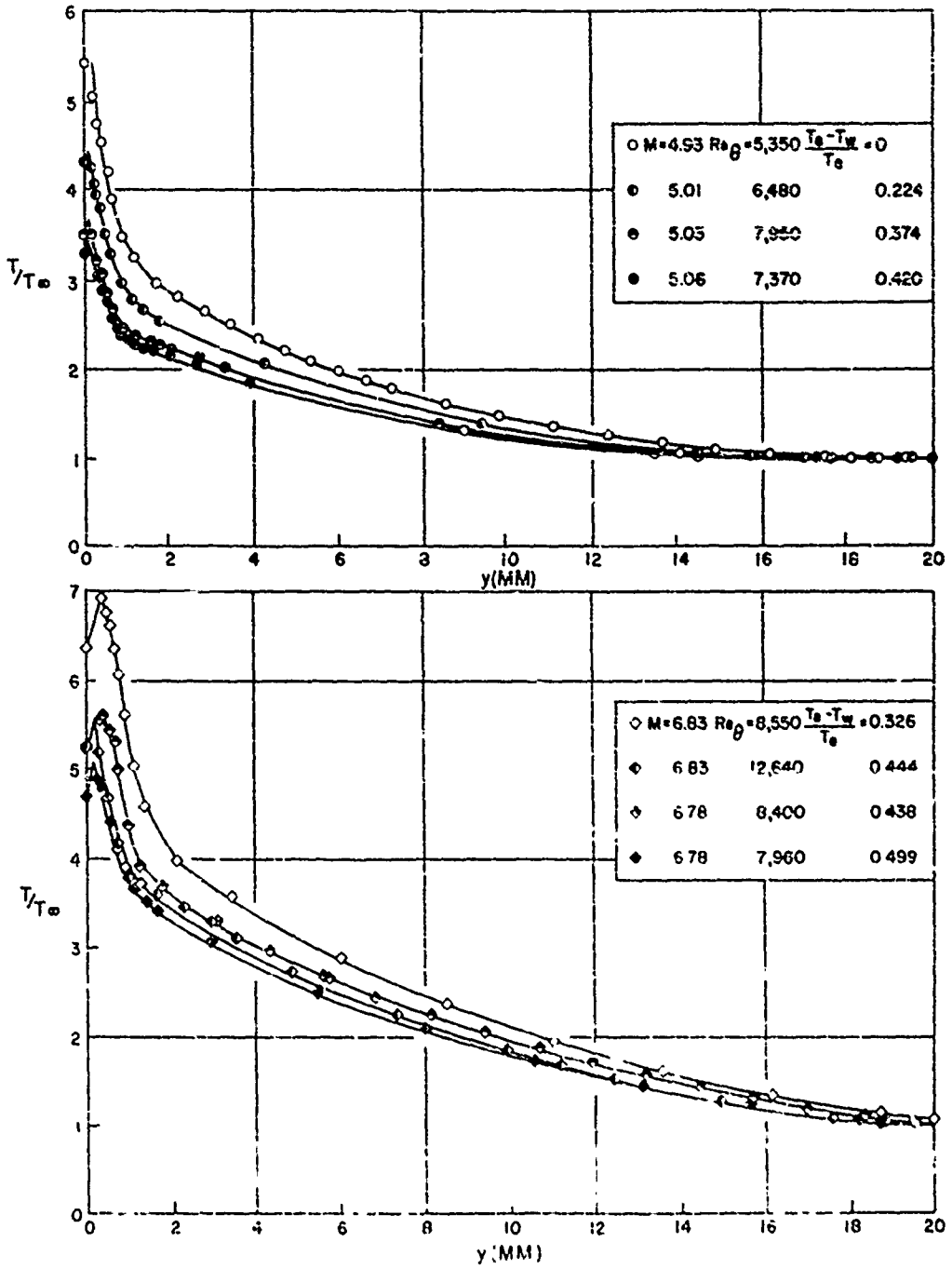

FIG 5 STATIC TEMPERATURE VARIATION ACROSS BOUNDARY LAYER FOR FREE-STREAM MACH NUMBERS OF 5 AND 6.8 AND VARIOUS RATES OF HEAT TRANSFER

VALUES BETWEEN 0<y<0.5 BASED ON INTERPOLATED T_t VALUES

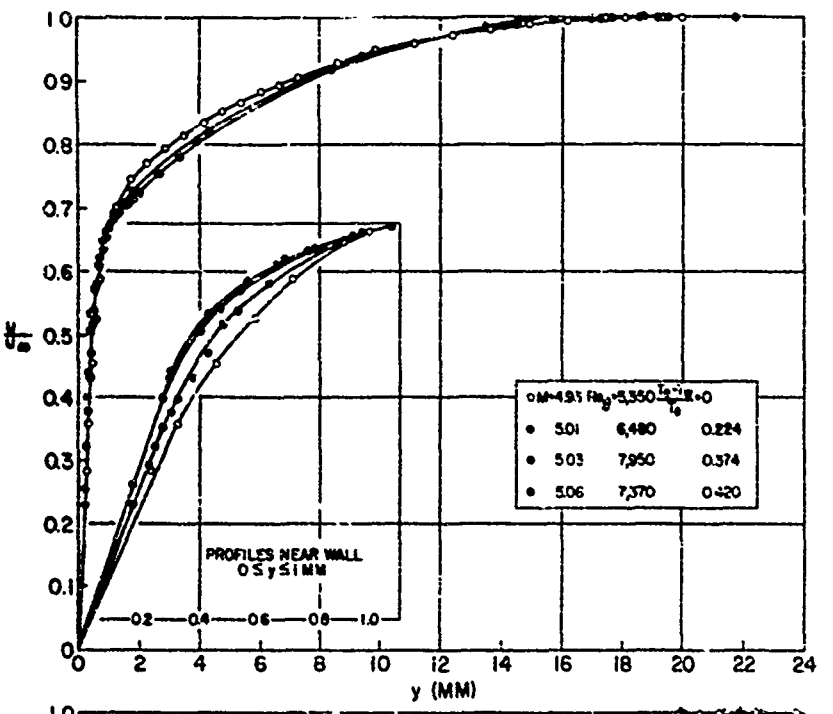

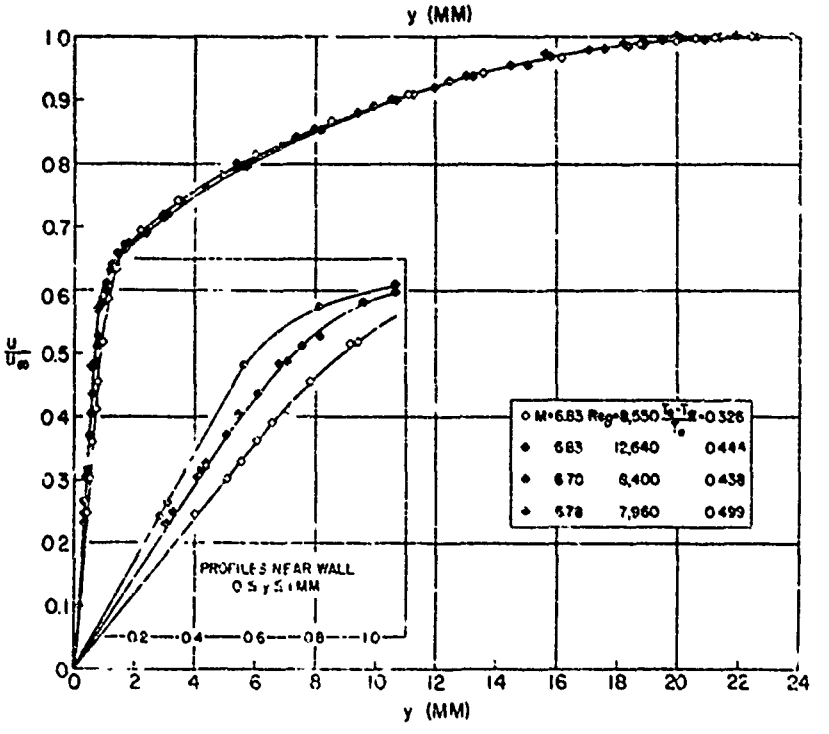

FIG. 6 VELOCITY VARIATION ACROSS BOUNDARY LAYER FOR FREE-STEAM MACH NUMBERS OF 5 AND 6.8 AND VARIOUS RATES OF HEAT TRANSFER

VALUES BETWEEN $0 < y < 0.5$ BASED ON INTERPOLATED T_t VALUES

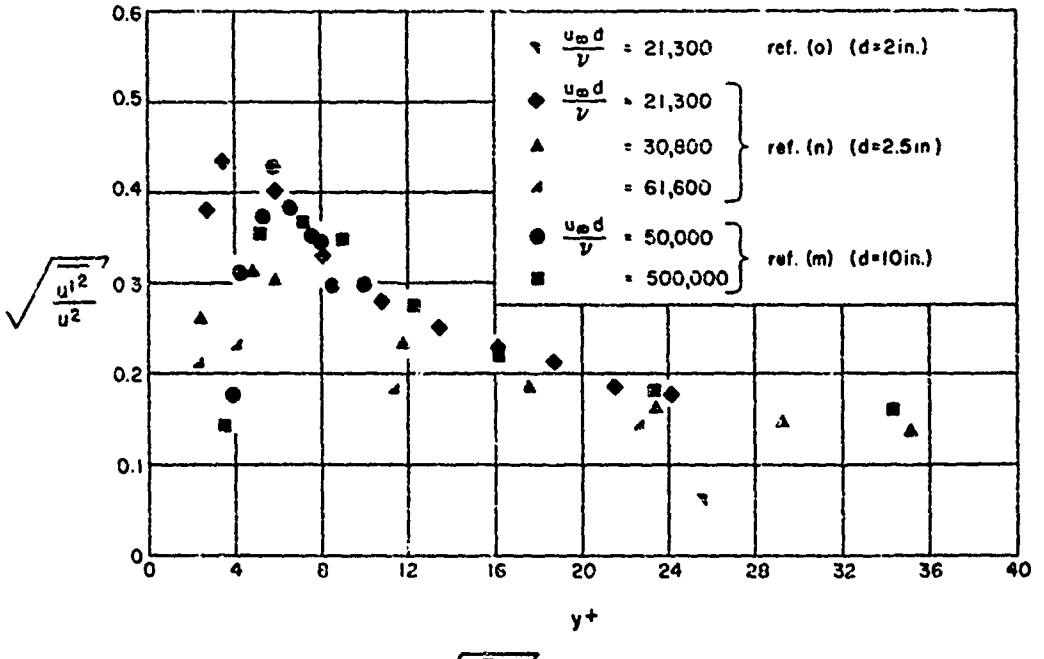

FIG. 7 VARIATION OF $\sqrt{\frac{\overline{u'^2}}{u^2}}$ WITH WALL DISTANCE PARAMETER (DATA FROM REFERENCES m, n AND o)

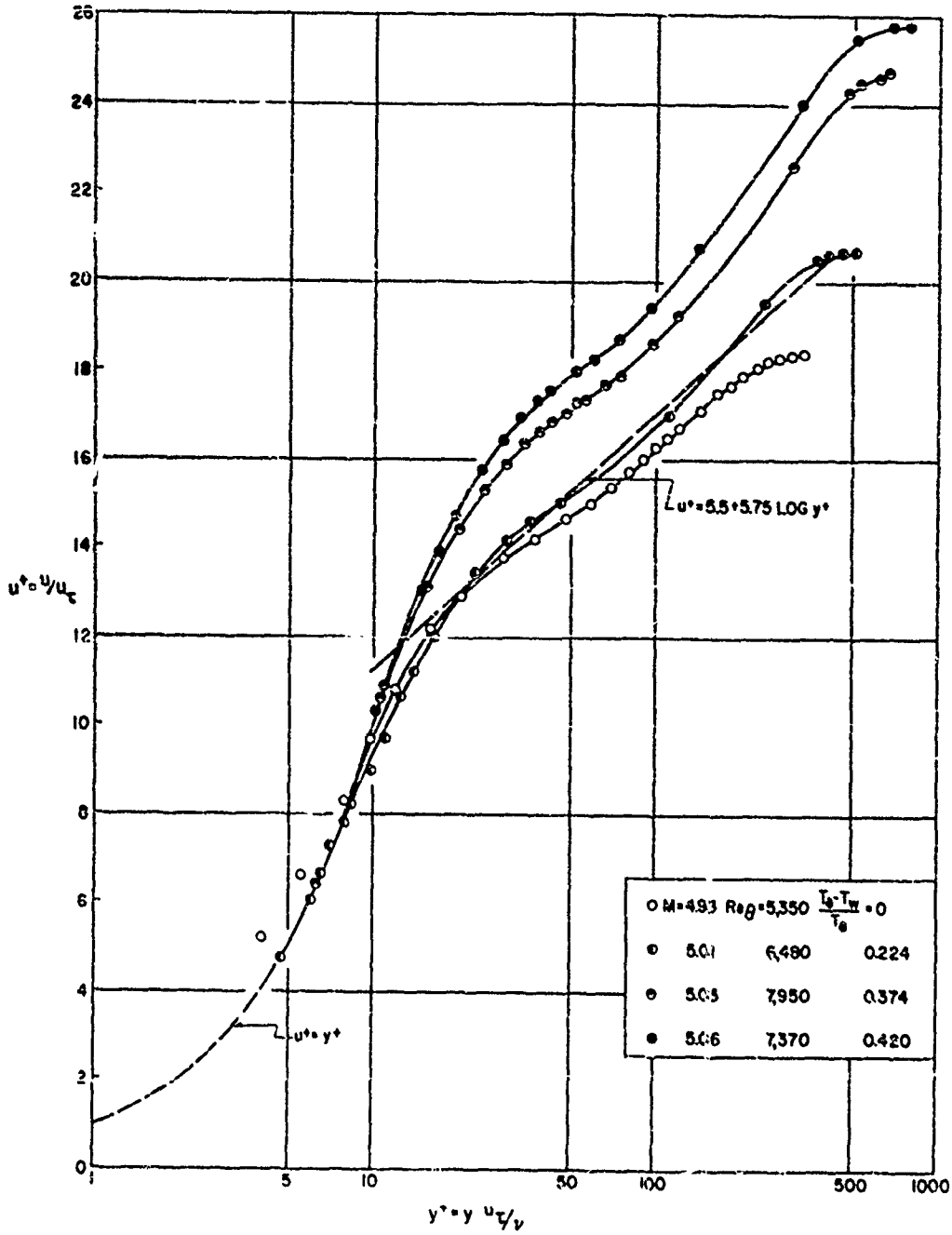

FIG 8 SEMI-LOGARITHMIC REPRESENTATION OF BOUNDARY LAYER VELOCITY PROFILES FOR A FREE-STREAM MACH NUMBER OF 5 AND FOUR RATES OF HEAT TRANSFER

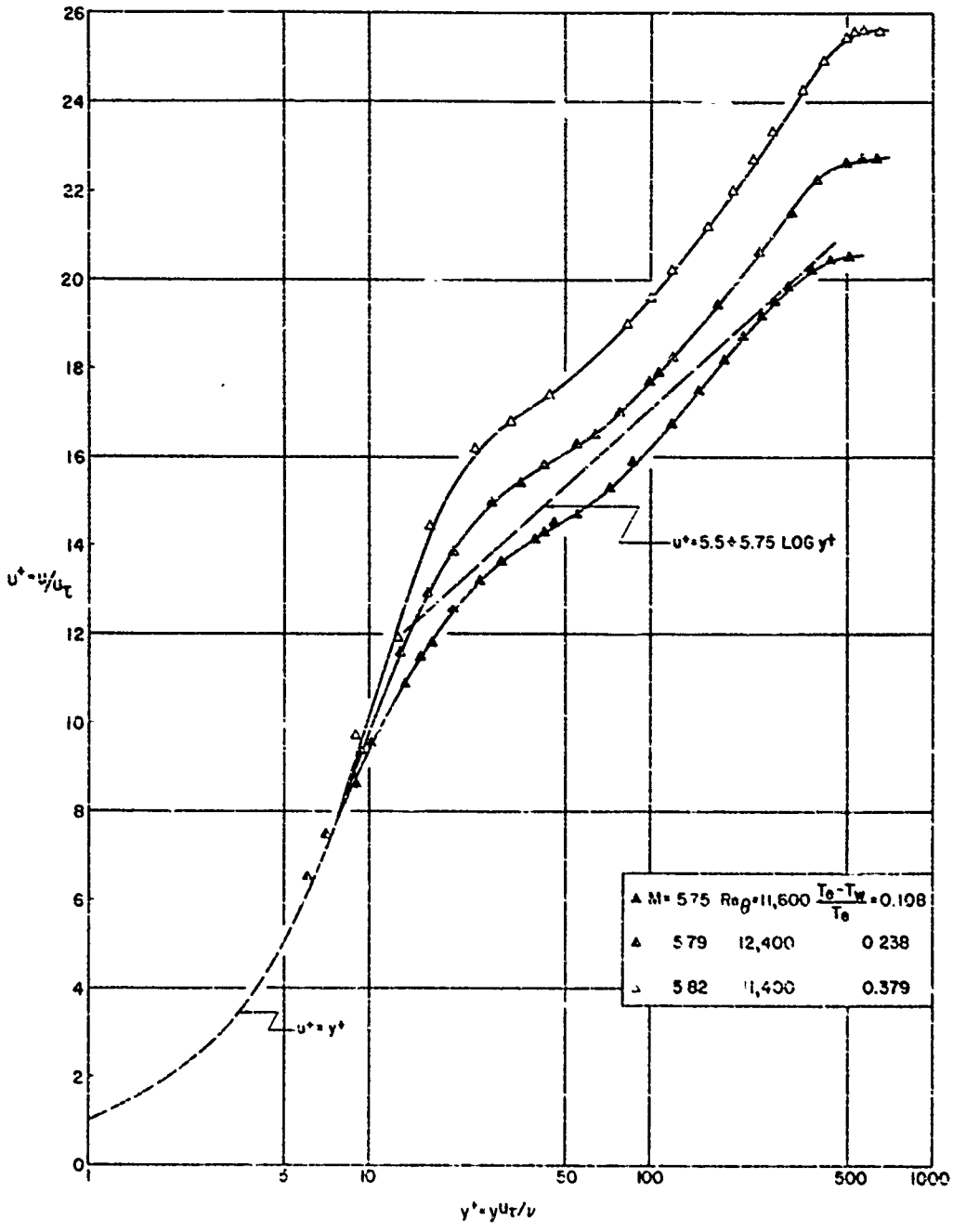

FIG. 9 SEMI-LOGARITHMIC REPRESENTATION OF BOUNDARY LAYER VELOCITY PROFILES FOR A FREE-STREAM MACH NUMBER OF 5.8 AND THREE RATES OF HEAT TRANSFER

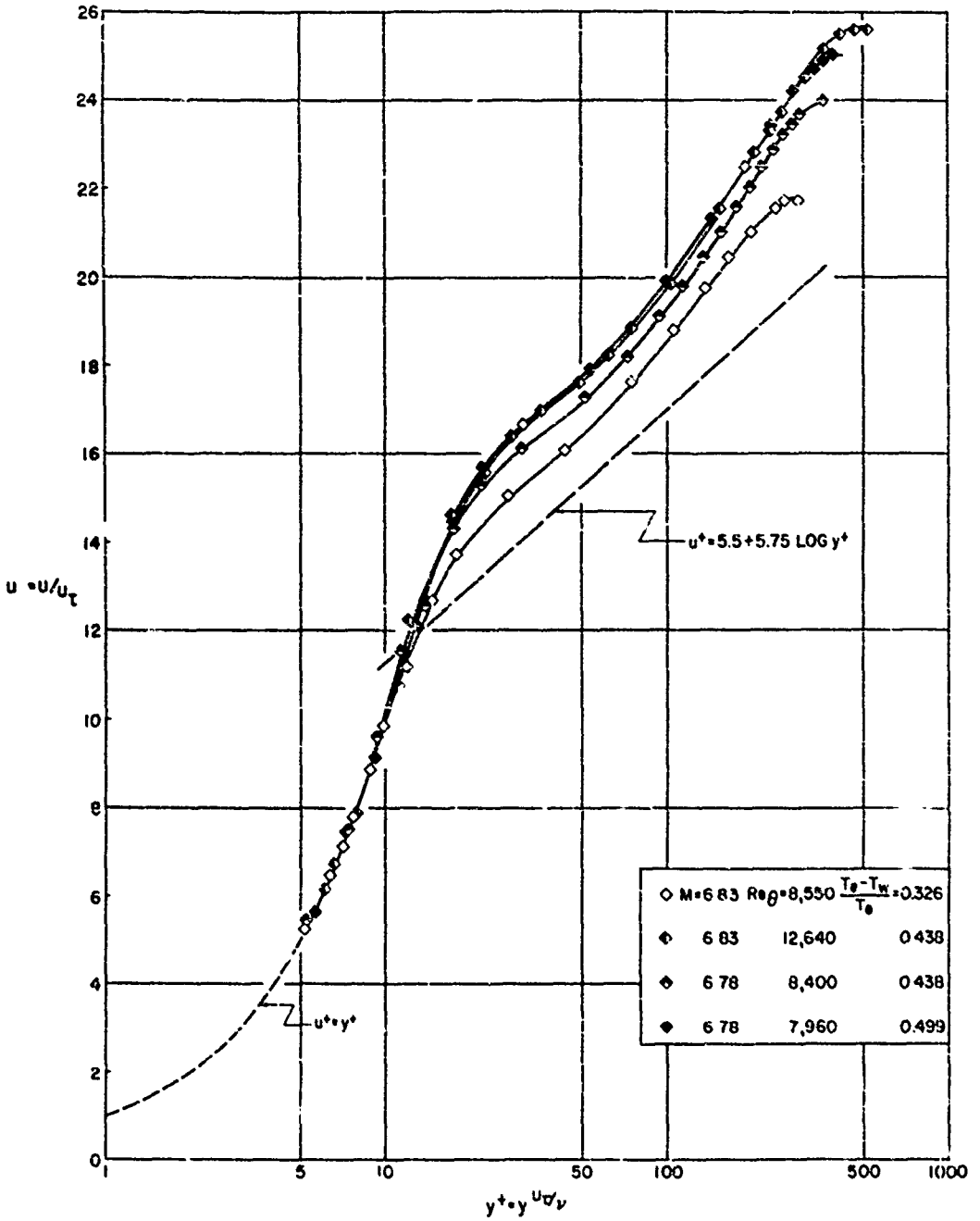

FIG 10 SEMI-LOGARITHMIC REPRESENTATION OF BOUNDARY LAYER VELOCITY PROFILES FOR A FREE-STREAM MACH NUMBER OF 6 8 AND FOUR RATES OF HEAT TRANSFER

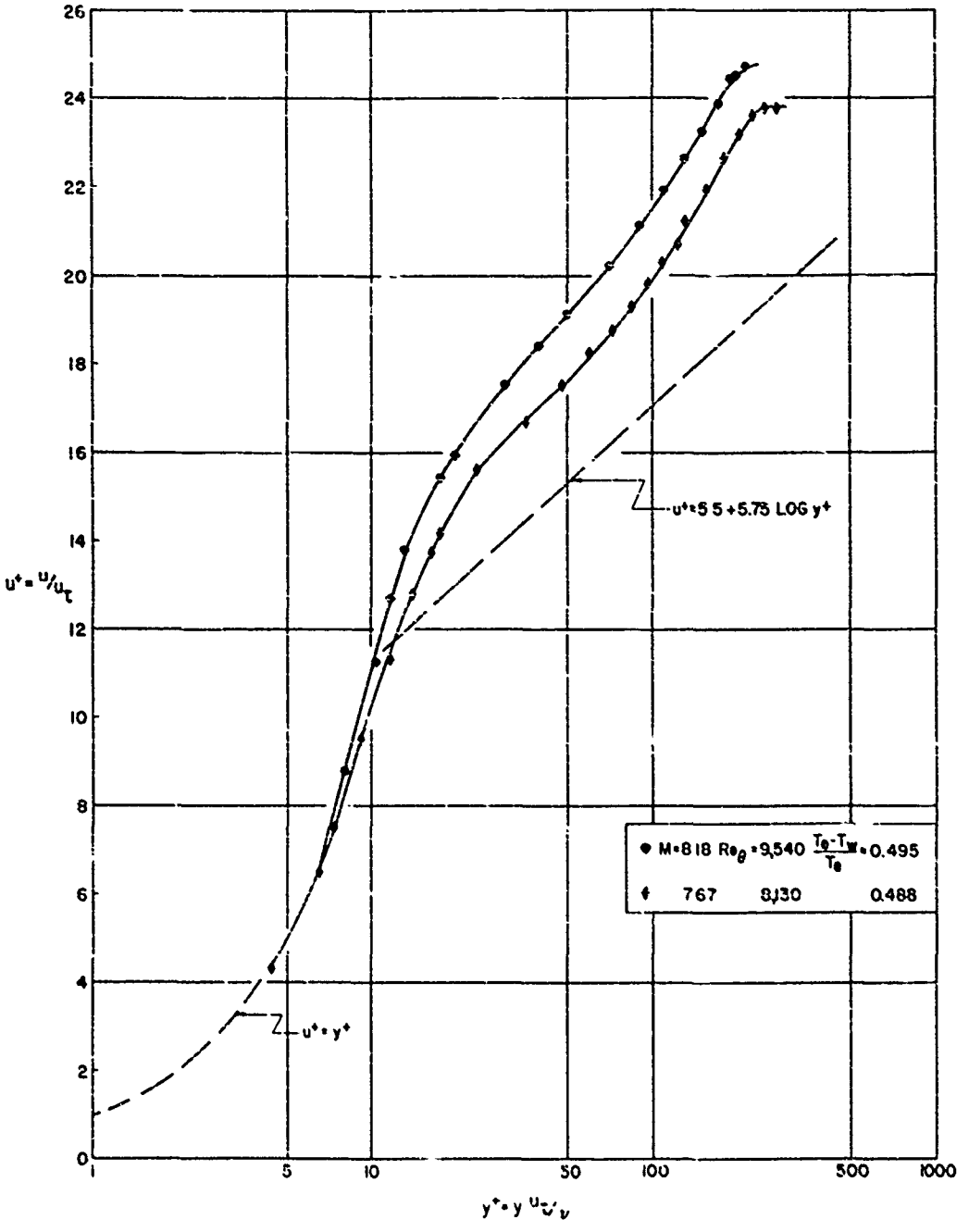

FIG. 11 SEMI-LOGARITHMIC REPRESENTATION OF BOUNDARY LAYER VELOCITY PROFILES FOR FREE-STREAM MACH NUMBERS OF 7.7 AND 8.2

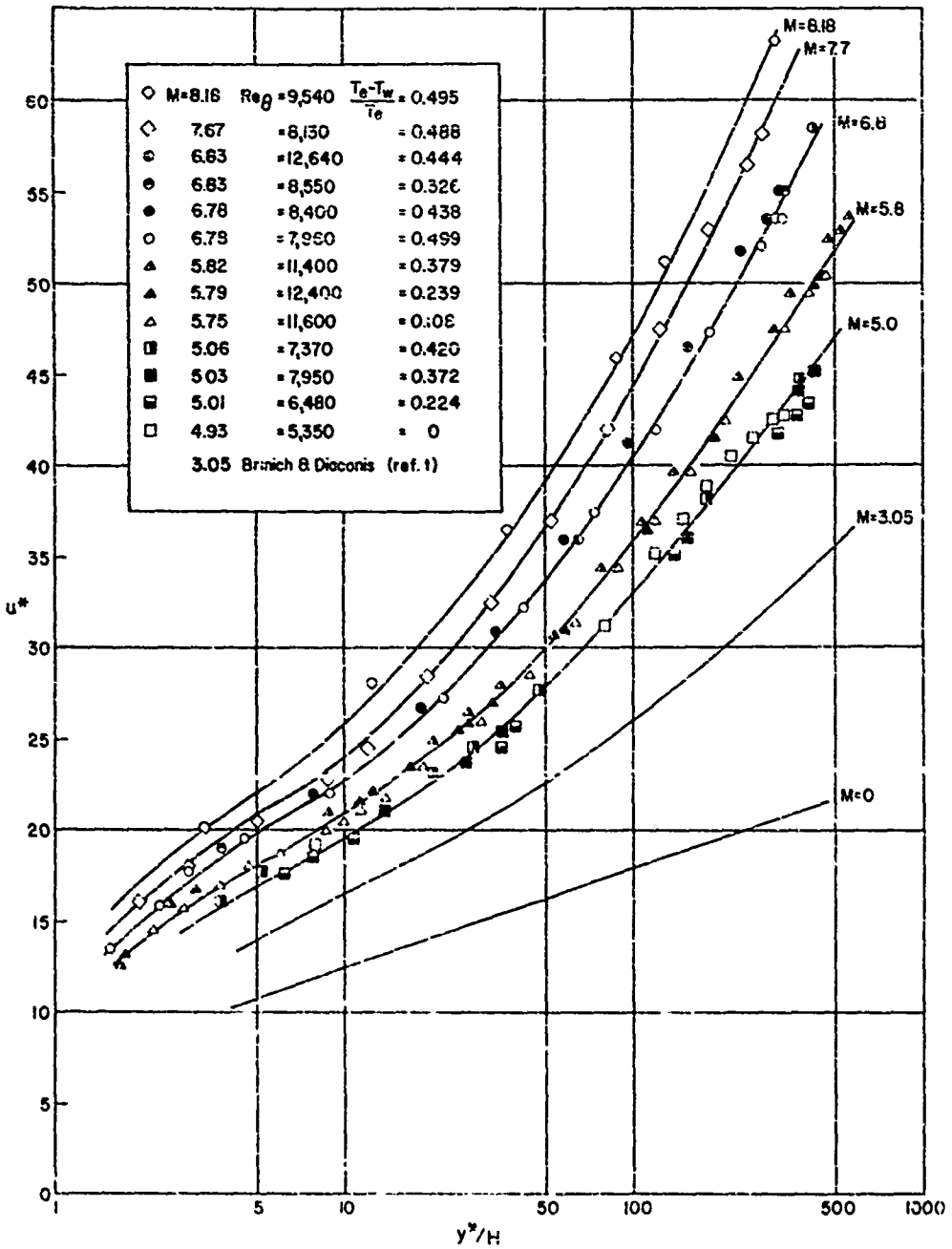

FIG. 12 SEMI-LOGARITHMIC REPRESENTATION OF TURBULENT PORTION OF BOUNDARY LAYER PROFILES IN u*, y*/H COORDINATES FOR VARIOUS MACH NUMBERS

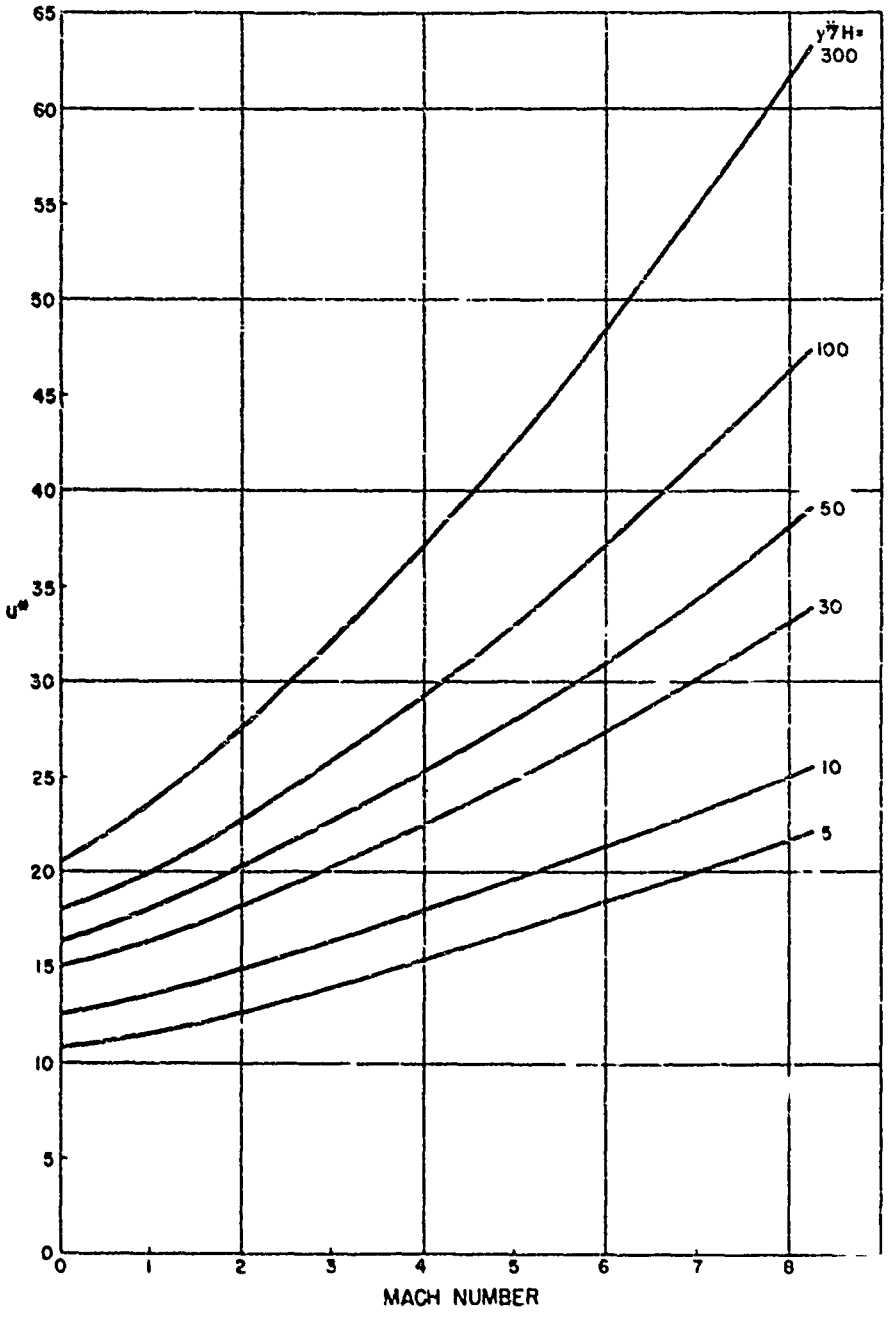

FIG. 13 VARIATION OF u* WITH MACH NUMBER FOR VARIOUS VALUES OF y*/H

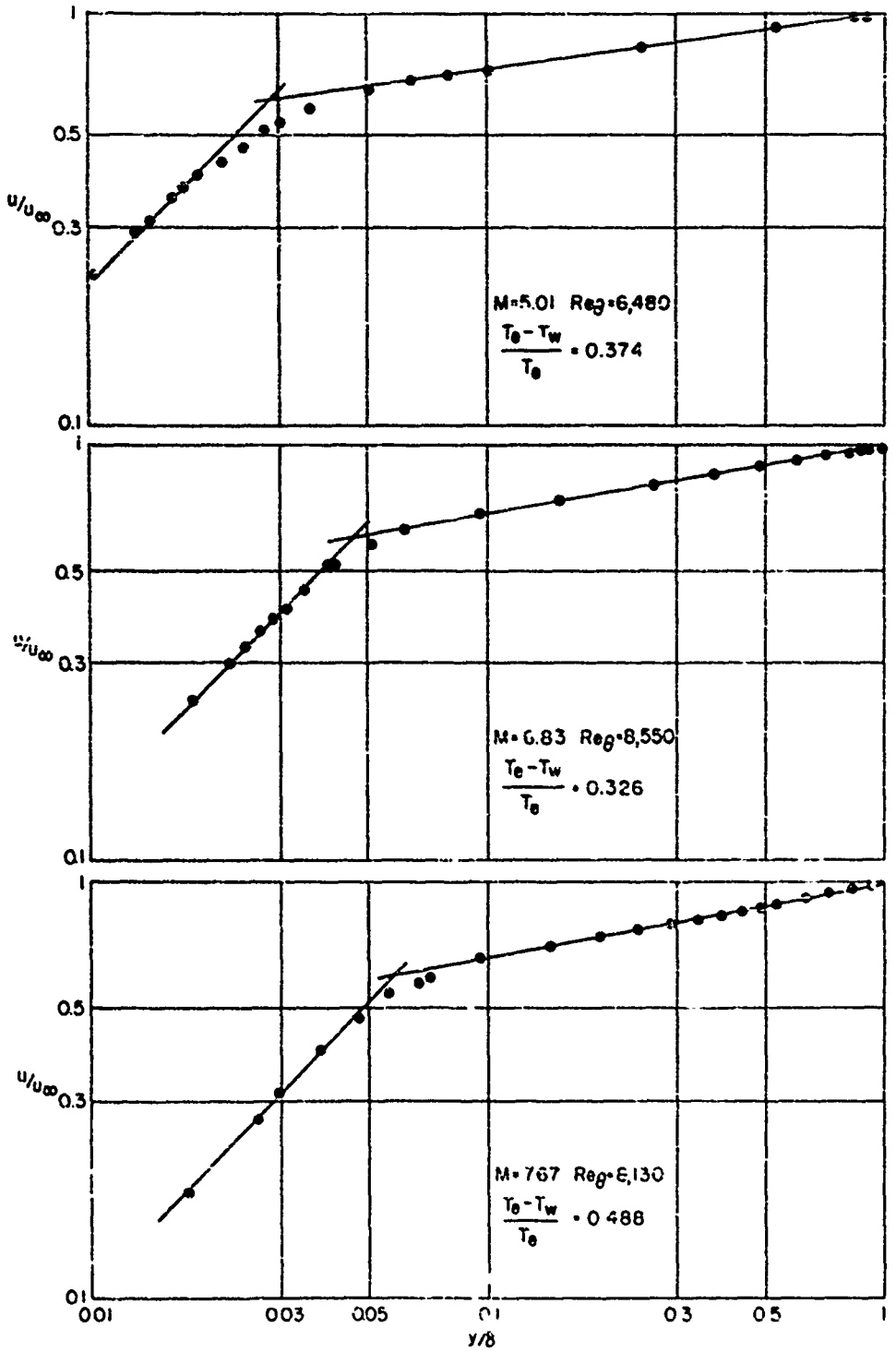

FIG 14 LOGARITHMIC REPRESENTATION OF BOUNDARY LAYER VELOCITY PROFILES

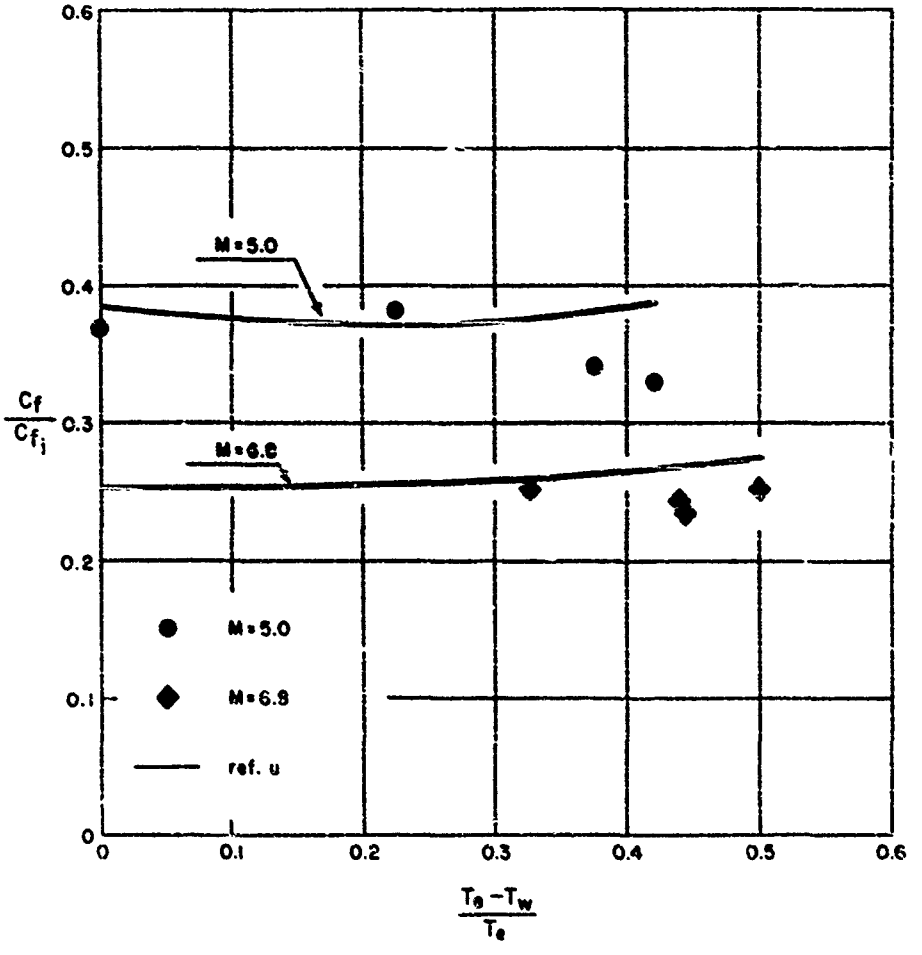

FIG.15 VARIATION OF SKIN FRICTION RATIO WITH HEAT TRANSFER PARAMETER

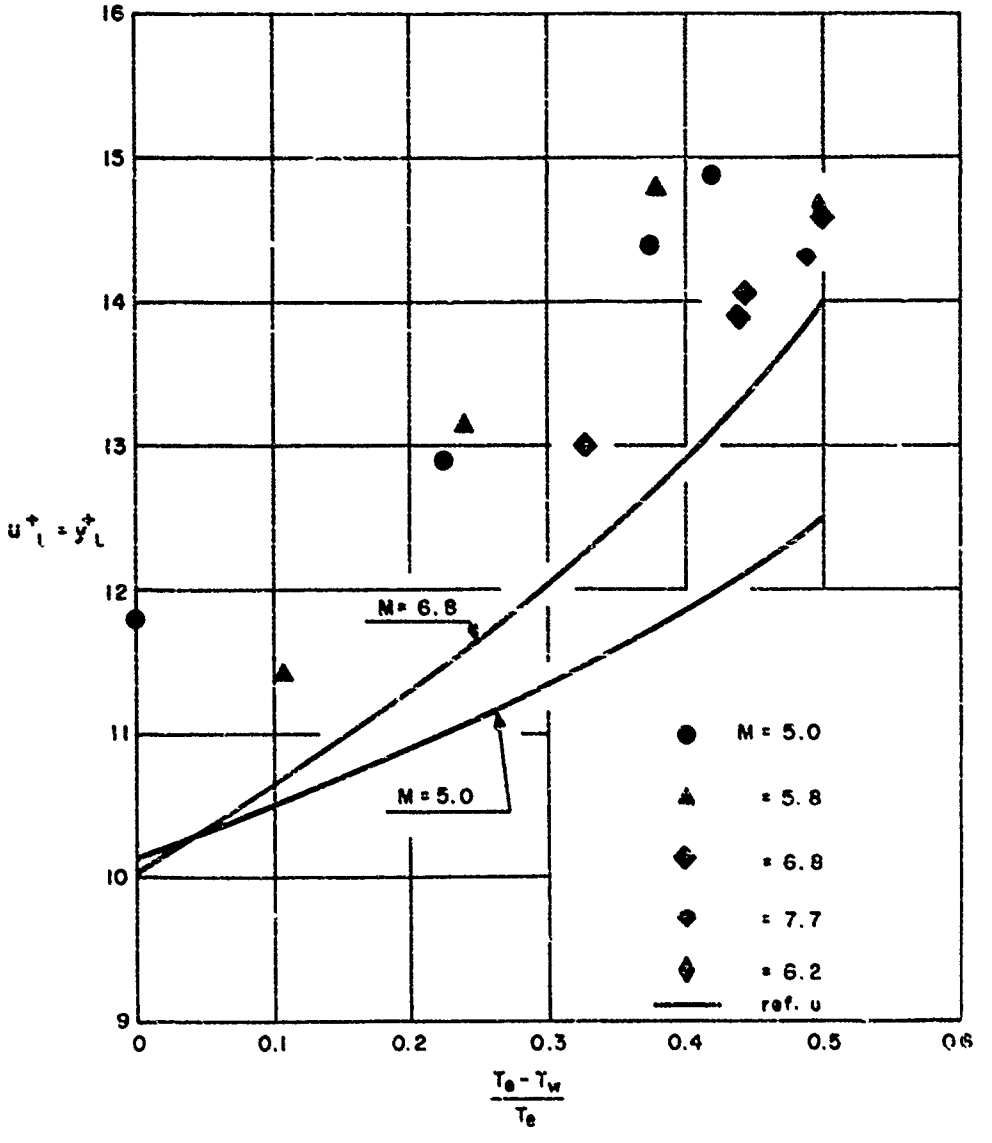

FIG.16 VARIATION OF $u^+_L = y^+_L$ VALUES WITH HEAT TRANSFER PARAMETER

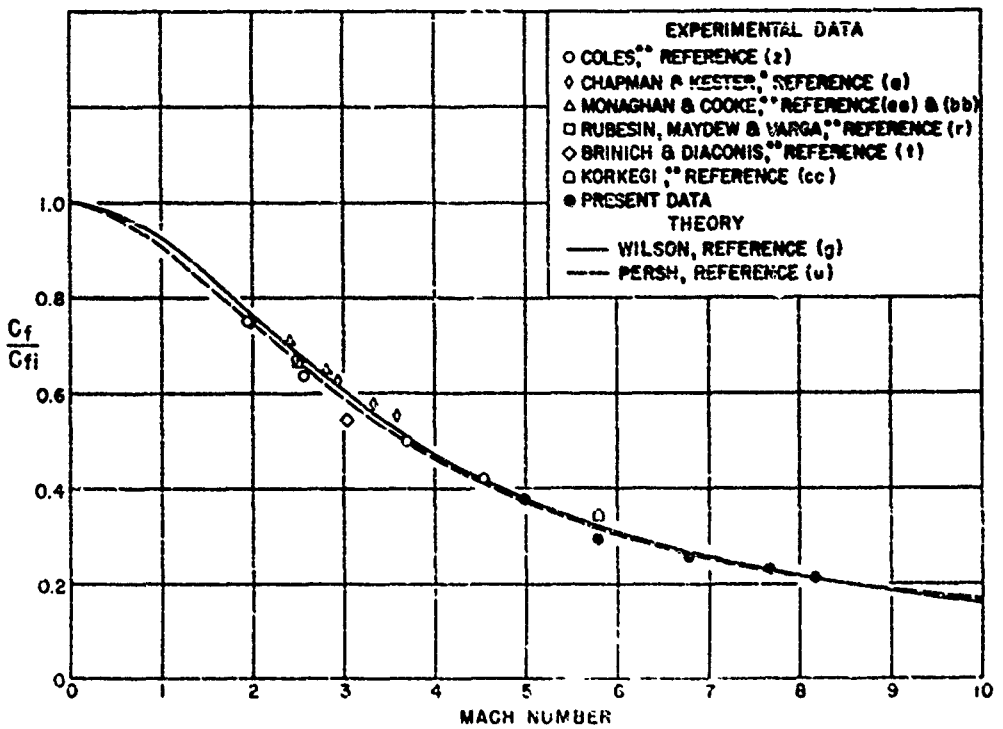

FIG.17 VARIATION OF SKIN FRICTION COEFFICIENT WITH MACH NUMBER FOR ZERO HEAT TRANSFER AND A Re_θ VALUE OF 8,000

* THE DATA PLOTTED ARE MEAN SKIN FRICTION RATIOS C_F/C_{Fi}
** THE DATA PLOTTED WERE OBTAINED FROM A STRAIGHT-LINE EXTRAPOLATION, RESPECTIVELY INTERPOLATION, OF C_f VS Re_θ

NAVORD Report 3880

Aeroballistic Research Department
External Distribution List for Aeroballistics Research (XI)

No. of Copies	
	Chief, Bureau of Ordnance Department of the Navy Washington 25, D. C.
1	Attn: Re3d
2	Attn: Re6
2	Attn: Re9a
	Chief, Bureau of Aeronautics Department of the Navy Washington 25, D. C.
1	Attn: AER-TD-414
2	Attn: RS-7
	Commander U. S. Naval Ordnance Test Station Inyokern P. O. China Lake, California
2	Attn: Technical Library
1	Attn: Code 5003
	Commander U. S. Naval Air Missile Test Center Point Mugu, California
2	Attn: Technical Library
	Superintendent U. S. Naval Postgraduate School Monterey, California
1	Attn: Librarian
	Commanding Officer and Director David Taylor Model Basin Washington 7, D. C.
2	Attn: Hydrodynamics Laboratory
	Chief of Naval Research Library of Congress Washington 25, D. C.
2	Attn: Technical Info. Div.
	Office of Naval Research Department of the Navy Washington 25, D. C.
1	Attn: Code 438
2	Attn: Code 463

No. of Copies	
	Director Naval Research Laboratory Washington 25, D. C.
1	Attn: Code 2021
1	Attn: Code 3800
	Office, Chief of Ordnance U. S. Army Washington 25, D. C.
1	Attn: ORDTU
2	Library Branch Research and Development Board Pentagon 3D1041 Washington 25, D. C.
	Chief, AFSWP P. O. Box 2610 Washington 25, D. C.
1	Attn: Technical Library
1	Chief, Physical Vulnerability Branch Air Targets Division Directorate of Intelligence Headquarters, USAF Washington 25, D. C.
	Commanding General Wright Air Development Center Wright-Patterson Air Force Base Dayton, Ohio
5	Attn: WCACD
1	Attn: WCSD
2	Attn: WCSOR
2	Attn: WCRRN
1	Attn: WCACD
1	Attn: WCRRF
2	Attn: WCLGH
1	Director Air University Library Maxwell Air Force Base, Alabama
	Commanding General Aberdeen Proving Ground Aberdeen, Maryland
1	Attn: C. L. Poor
1	Attn: D. S. Dederick

No. of Copies	
	National Bureau of Standards Washington 25, D. C.
1	Attn: Nat'l Applied Math. Lab.
1	Attn: Librarian (Ord. Dev. Div.)
1	Attn: Chief, Mechanics Div.
	National Bureau of Standards Corona Laboratories (Ord. Dev. Div.) Corona, California
1	Attn: Dr. H. Thomas
	University of California 211 Mechanics Building Berkeley 4, California
1	Attn: Mr. G. J. Maslach
1	Attn: Dr. S. A. Schaaf
2	Commanding General Redstone Arsenal Huntsville, Alabama Attn: Tech. Library
1	Jet Propulsion Lab. California Institute of Technology 4800 Oak Grove Drive Pasadena 3, California Attn: F. E. Goddard, Jr.
	California Institute of Technology Pasadena 4, California
2	Attn: Librarian (Guggenheim Aero Lab)
1	Attn: Dr. H. T. Nagamatsu
1	Attn: Prof. M. S. Plesset
1	Attn: Dr. Hans W. Liepmann VIA: BuAer Representative
	University of Illinois 202 E. E. R. L. Urbana, Illinois
1	Attn: Prof. A. H. Taub
1	Director Inst. for Fluid Dynamics and Applied Math University of Maryland College Park, Maryland
	Massachusetts Inst. of Technology Cambridge 39, Massachusetts
1	Attn: Prof. G. Stever
1	Attn: Prof. J. Kaye

No. of Copies	
	University of Michigan Ann Arbor, Michigan
1	Attn: Prof. Otto Laporte
	University of Michigan Willow Run Research Center Ypsilanti, Michigan
1	Attn: L. R. Biasell
	Dept. of Mechanical Engr. University of Minnesota Institute of Technology Minneapolis 14, Minnesota
1	Attn: Prof. N. A. Hall
	The Ohio State University Columbus, Ohio
2	Attn: G. L. Von Eschen
	Polytechnic Institute of Brooklyn Aerodynamics Laboratory 527 Atlantic Avenue Freeport, New York
1	Attn: Dr. Antonio Ferri VIA: ONR
	Princeton University Princeton, New Jersey
1	Attn: Prof. S. Bogdonoff VIA: ONR
	Massachusetts Inst. of Technology Cambridge 39, Massachusetts
2	Attn: Project Meteor
1	Attn: Guided Missiles Library
1	Princeton University Forrestal Research Center Library Project Squid Princeton, New Jersey
	Armour Research Foundation 35 West 33rd Street Chicago 16, Illinois
1	Attn: Engr. Mech. Div. VIA: ONR

No. of Copies

Applied Physics Laboratory
The Johns Hopkins University
8621 Georgia Avenue
Silver Spring, Maryland
1 Attn: Arthur G. Norris
VIA: NIO

1 Cornell Aeronautical Lab., Inc.
4455 Genesee Street
Buffalo 21, New York
VIA: BuAer Rep.

1 Defense Research Laboratory
University of Texas
Box 1, University Station
Austin, Texas

Eastman Kodak Company
50 W. Main Street
Rochester 4, New York
1 Attn: Dr. Herbert Trotter, Jr.
VIA: NIO

General Electric Company
Building #1, Campbell Ave. Plant
Schenectady, New York
1 Attn: Joseph C. Hoffman
VIA: InsMachinery

The Rand Corporation
1700 Main Street
Santa Monica, California
1 Attn: The Librarian

Consolidated Vultee Aircraft Corp.
Daingerfield, Texas
1 Attn: J. E. Arnold
VIA: Dev. Contract Office

Douglas Aircraft Company, Inc.
3000 Ocean Park Boulevard
Santa Monica, California
1 Attn: Mr. E. F. Burton
VIA: Bu Aer Resident Rep.

1 BuAer Representative
AeroJet--General Corp.
6352 North Irwindale Ave.
Azusa, California

No. of Copies	
	North American Aviation, Inc. 12214 Lakewood Boulevard Downey, California
2	Attn: Aerophysics Library VIA: BuAer Representative
	United Aircraft Corporation East Hartford 8, Connecticut
1	Attn: Robert C. Sale VIA: BuAer Representative
	National Advisory Committee for Aero. 1512 H Street, Northwest Washington 25, D. C.
5	Attn: E. B. Jackson
	Ames Aeronautical Laboratory Moffett Field, California
1	Attn: H. J. Allen
2	Attn: Dr. A. C. Charters
	NACA Lewis Flight Propulsion Lab Cleveland Hopkins Airport Cleveland 11, Ohio
1	Attn: John C. Evvard
	Langley Aeronautical Laboratory Langley Field, Virginia
1	Attn: Theoretical Aerodynamics Div.
1	Attn: J. V. Becker
1	Attn: Dr. Adolf Buseman
1	Attn: Mr. C. H. McLellan
1	Attn: Mr. J. Stack
	Harvard University 21 Vanserg Building Cambridge 38, Massachusetts
1	Attn: Prof. Garrett Birkhoff
	The Johns Hopkins University Charles and 34th Streets Baltimore 18, Maryland
1	Attn: Dr. Francis H. Clauser
	New York University 45 Fourth Avenue New York 3, New York
1	Attn: Professor R. Courant

No. of Copies

1 Dr. Allen E. Puckett, Head
Missile Aerodynamics Department
Hughes Aircraft Company
Culver City, California

1 Dr. Gordon N. Patterson, Director
Institute of Aerophysics
University of Toronto
Toronto 5, Ontario, Canada
VIA: BuOrd (Ad8)

Acroon, Inc.
385 E. Green Street
Pasadena 1, California
1 VIA: Inspector of Naval Mat'l
1206 S. Santeo Street
Los Angeles 15. Calif.

Engineering Research Inst.
East Engineering Building
1 Ann Arbor, Michigan
Attn: Director of Icing Research

Aeroballistic Research Department
External Distribution List for Aeroballistics Research (XIa)

No. of Copies	
6	Office of Naval Research Branch Office Navy 100 Fleet Post Office New York, New York
	Commanding General Aberdeen Proving Ground Aberdeen, Maryland
1	Attn: Dr. B. L. Hicks
	National Bureau of Standards Aerodynamics Section Washington 25, D. C.
1	Attn: Dr. G. B. Schubauer, Chief
	Ames Aeronautical Laboratory Moffett Field, California
1	Attn: Walter G. Vincenti
	University of California Observatory 21 Berkeley 4, California
1	Attn: Leland E Cunningham
	Massachusetts Inst. of Technology Dept. of Mathematics, Room 2-270 77 Massachusetts Avenue Cambridge, Massachusetts
1	Attn: Prof. Eric Reissner
	Graduate School Aeronautical Engr. Cornell University Ithaca, New York
1	Attn: W. R. Sears, Director VIA: ONR
	Applied Math. and Statistics Lab. Stanford University Stanford, California
1	Attn: R. J. Langle, Associate Dir.
	University of Minnesota Dept. of Aeronautical Engr. Minneapolis, Minnesota
1	Attn: Professor R. Hermann

No. of Copies

1 Dr. Allen E. Puckett, Head
Missile Aerodynamics Department
Hughes Aircraft Company
Culver City, California

1 Dr. Gordon N. Patterson, Director
Institute of Aerophysics
University of Toronto
Toronto 5, Ontario, Canada
VIA: BuOrd (Ad8)

Acroon, Inc.
385 E. Green Street
Pasadena 1, California
1 VIA: Inspector of Naval Mat'l
1206 S. Santeo Street
Los Angeles 15, Calif.

Engineering Research Inst.
East Engineering Building
1 Ann Arbor, Michigan
Attn: Director of Icing Research

Aeroballistic Research Department
External Distribution List for Aeroballistics Research (XIa)

No of Copies	
6	Office of Naval Research Branch Office Navy 100 Fleet Post Office New York, New York
	Commanding General Aberdeen Proving Ground Aberdeen, Maryland
1	Attn: Dr. B. L. Hicks
	National Bureau of Standards Aerodynamics Section Washington 25, D. C.
1	Attn: Dr. G. B. Schubauer, Chief
	Ames Aeronautical Laboratory Moffett Field, California
1	Attn: Walter G. Vincenti
	University of California Observatory 21 Berkeley 4, California
1	Attn: Leland E. Cunningham
	Massachusetts Inst. of Technology Dept. of Mathematics, Room 2-270 77 Massachusetts Avenue Cambridge, Massachusetts
1	Attn: Prof. Eric Reissner
	Graduate School Aeronautical Engr. Cornell University Ithaca, New York
1	Attn: W. R. Sears, Director VIA: ONR
	Applied Math. and Statistics Lab. Stanford University Stanford, California
1	Attn: R. J. Langle, Associate Dir.
	University of Minnesota Dept of Aeronautical Engr. Minneapolis, Minnesota
1	Attn: Professor R. Hermann

No. of
Copies

Case Institute of Technology
Dept. of Mechanical Engineering
Cleveland, Ohio
1 Attn: Professor G. Kuerti
VIA: ONR

Harvard University
109 Pierce Hall
Cambridge 38, Massachusetts
1 Attn: Professor R. von Mises

EXTERNAL DISTRIBUTION

No. of Copies	
1	Mr. A. I. Moskovitz Bureau of Ordnance (Re9a) Navy Department Washington, D. C.
1	Chief, Naval Operations Department of the Navy Washington 25, D. C.
1	The Artillery School Anti-aircraft & Guided Missiles Br. Fort Bliss, Texas Attn: Research & Analysis Sec.
1	Dr. K. F. Rubert Internal Aerodynamics Branch National Advisory Committee for Aeronautics Langley Field, Virginia
1	Prof. R. F. Probstein Division of Engineering Brown University Providence, Rhode Island
1	Commander U. S. Naval Proving Ground Dahlgren, Virginia
1	Jet Propulsion Laboratory 4800 Oak Grove Drive Pasadena, California Attn: Dr. P. P. Wegener
1	Flight and Aerodynamics Laboratory Research Division Ordnance Missile Laboratory Redstone Arsenal Huntsville, Alabama Attn: J. L. Potter, Chief
5	U. S. Air Force Headquarters Arnold Engineering Development Center (ARDC) Tullahoma, Tennessee Attn: AEKS
1	Dr. R. H. Mills Wright Air Development Center Wright-Patterson Air Force Base Dayton, Ohio

No. of
Copies

1 Mr. Ronald Smelt
Chief, Gas Dynamics Facility
Arnold Research Organization, Inc.
Tullahoma, Tennessee

1 Dr. Henry Nagamatsu
California Institute of Technology
Pasadena, California

1 Professor N. J. Hoff
Polytechnic Institute of Brooklyn
Brooklyn, New York

1 Dr. F. L. Wattendorf
Facilities Division DCS/Development
Hdqts. USAF, Room 5C368
Pentagon, Washington 25, D. C.

1 Professor A. Kantrowitz
Cornell University
Department of Aeronautical Engineering
Ithaca, New York

1 Professor Lester Lees
California Institute of Technology
Pasadena, California

1 Dr. H. G. Stever
MIT, Department of Aeronautical Engineering
Cambridge, Massachusetts

1 Professor G. L. Von Eschen
Aeronautical Engineering Department
Ohio State University
Columbus, Ohio

1 Mr. R. L. Bayless
Consolidated Vultee Aircraft Corporation
San Diego, California

1 Professor S. M. Bogdonoff
Department of Aeronautical Engineering
Princeton University
Princeton, New Jersey

1 Professor J. Kaye
MIT, Physics Department
Cambridge, Massachusetts

No. of
Copies

1 Dr. Ernst R. G. Eckert
Department of Mechanical Engineering
University of Minnesota
Minneapolis 14, Minnesota

1 Mr. Mervin Sibulkin
Jet Propulsion Laboratory
4800 Oak Grove Drive
Pasadena, California

1 Dr. G. R. Boer
Holloman Air Force Base
Alamagordo, New Mexico

1 Dr. Albert E. Lombard
Pentagon, Rm. 4E348
Washington, D. C.

1 Dr. E. R. Van Driest
Aerophysics Laboratory
North American Aviation, Inc.
Downing, California

1 Dr. Paul A. Libby
Polytechnic Institute of Brooklyn
99 Livingston Street
Brooklyn, New York

1 Dr. W. S. Bradfield
Aero. Engr. Dept.
University of Minnesota
Minneapolis, Minnesota

1 Dr. D. Coles
California Institute of Technology
Pasadena 4, California

1 Prof. Dr. H. Reichardt
Max Planck Institut fuer Stroemungsforschung
Goettingen, Germany

1 Prof. Dr. H. Schlichting
Institut fuer Stroemungsmechanik der
Technischen Hochschule
Wodanstrasse 42
Braunschweig, Germany

1 Prof. Dr J. Ackeret
Soenneggstrasse 3
Zurich 6, Switzerland

No. of Copies	
1	D. N. Morris Douglas Aircraft Company, Inc. El Segundo Division El Segundo, California
1	K. E. Van Every Douglas Aircraft Company, Inc. El Segundo Division El Segundo, California
1	Dr. G. V. Bull Canadian Armament Research and Development Establishment P. O. Box 1427 Quebec, Quebec, Canada
2	Dr. Philip A. Hufton Aeronautical Department Royal Aircraft Establishment Farnborough, England
1	Paul F. Brinich NACA, Lewis Flight Propulsion Laboratory Cleveland 11, Ohio
1	Dr. I. I. Glass Institute of Aerophysics University of Toronto Toronto 5, Ontario, Canada
1	Prof. H. F. Ludloff Daniel Guggenheim School of Aeronautics New York University New York 3, New York
1	John Laufer Jet Propulsion Laboratory California Institute of Technology 4800 Oak Grove Drive Pasadena 2, California
1	William H. Dorrance Consolidated Vultee Aircraft Corporation San Diego, California
1	Professor Dean MIT, Gas Turbine Laboratory Engineering Department Cambridge, Massachusetts

No. of
Copies

1 Major J. B. Robinson
U. S. Air Force
Main Navy Building, Rm. 3816
Washington 25, D. C.

1 D. R. Bartz
Jet Propulsion Laboratory
California Institute of Technology
4800 Oak Grove Drive
Pasadena 3, California

1 William F. Brown
Los Alamos Scientific Laboratory
University of California
P. O. Box 1663
Los Alamos, New Mexico

1 P. S. Klebanoff
Aerodynamic Section
National Bureau of Standards
Washington 25, D. C.

1 Judson Baron
Naval Supersonic Laboratory
Massachusetts Institute of Technology
Cambridge, Massachusetts

1 Marvin Sweeney, Jr.
Naval Supersonic Laboratory
Massachusetts Institute of Technology
Cambridge, Massachusetts

1 Dr. F. Frenkiel
Applied Physics Laboratory
The Johns Hopkins University
8621 Georgia Avenue
Silver Spring, Maryland

1 Dr. F. K. Hill
Applied Physics Laboratory
The Johns Hopkins University
8621 Georgia Avenue
Silver Spring, Maryland

1 Mr. E. A. Bonney
Applied Physics Laboratory
The Johns Hopkins University
8621 Georgia Avenue
Silver Spring, Maryland

No. of Copies	
1	Dr. Francis R. Institute of F University of College Park,
1	Prof. S. F. Sh Aeronautical E University of College Park,
1	Prof. S. I. Pa Institute of F University of College Park,
1	Dr. William Bo Aerophysics De 15304 Sunset B Pacific Palisa
1	Dr. D. R. Chap NACA, Ames Aero Moffett Field,
1	Alvin Seiff NACA, Ames Aero Moffett Field,
1	Morris W. Rubes NACA, Ames Aero Moffett Field,
1	R. G Deissler NACA, Lewis Fli Cleveland 11, O
1	Col . Du P. D Ae nautical En Princeton Unive Princeton, New
1	R. J. Monaghan Aeronautical De Royal Aircraft Farnborough, En
1	Satish Dhawan California Inst Pasadena 4, Cal